DRDC Toronto CR 2005-115

Development of a Dynamic Biomechanical Model for Load Carriage: Phase I Part A:

Equipment Upgrades to Accommodate Dynamic Biomechanical Modeling

by:
Joan M. Stevenson, Ph.D. , Susan A. Reid, M.Sc., P.Eng., J. Tim Bryant, Ph.D., P.Eng.,
Lindsay J. Hadcock, B.Sc, P.Eng., and Evelyn L. Morin, Ph.D., P.Eng.

Ergonomics Research Group
School of Physical and Health Education
Queen's University, Kingston, Ontario K7L 3N6

Project Manager:
J.M. Stevenson, Ph.D.
(613) 545-6288

PWGSC TIES Contract # W7711-0-7632-01 /A
on behalf of
DEPARTMENT OF NATIONAL DEFENCE

as represented by
Defence Research and Development Canada - Toronto
1133 Sheppard Avenue West
North York, Ontario, Canada
M3M 3B9

DRDC Scientific Authority:
Maj Linda Bossi
(416) 635-2197

August 2005

Abstract

Part A of Phase I of the contract was to develop the instrumentation so that a dynamic biomechanical model could be developed. The specific objectives were: a) to develop Fastrak™ software for relative pack-person motion, b) construct smaller strap force gauges, c) build and calibrate a moment of inertia platform, d) modify the Load Carriage compliance tester to automate two degrees of freedom and e) create a full body mapping of mannequin. This report describes the purposes and outputs available from the pack-person motion (Section 2.0), describes the development, construction, calibration and protocol for use of smaller strap sensors (Section 3.0) and the moment of inertia platform (Section 4.0), and the development and steps involved in modifying the LC compliance tester (Section 5.0) and the mannequin mapping (Section 6.0). For the most part, tasks were developmental and construction-based with no data analyses, other than to confirm the accuracy and precision of the instrumentation.

This report deals only with Part A consisting of five sub-parts of the contract. Part B involved changing the technical manuals based on the upgrades stated within this report. Part C of this contract is under separate cover and was to develop a long range plan and budget for dynamic biomechanical modeling. Part D was to assist with the NATO HFM Specialist Meeting entitled “Soldier Mobility: Innovations in Load Carriage System Design and Evaluation” held on 27-29 June 2000. Part D is described by the NATO RTO MP-56 Technical Proceedings Report entitled: “Soldier Mobility: Innovations in Load Carriage System Design and Evaluation”.

Résumé

La partie A de la phase I du contrat avait pour but la mise au point d'instruments afin de permettre l'élaboration d'un modèle biomécanique dynamique. Elle visait les objectifs précis suivants : a) développer le logiciel Fastrak^{mc} afin de déterminer le mouvement relatif entre un sac à dos et une personne, b) construire de plus petits dynamomètres de sangle, c) fabriquer et étalonner une plate-forme de moment d'inertie, d) modifier l'appareil d'essai de conformité de transport tactique afin d'automatiser 2 degrés de liberté et e) créer une représentation intégrale du corps du mannequin. Le présent rapport décrit la raison d'être du logiciel et de ses sorties relativement au mouvement entre le sac à dos et la personne (section 2.0); la mise au point, la fabrication, l'étalonnage et le protocole d'utilisation de plus petits capteurs de sangle (section 3.0) ainsi que de la plate-forme de moment d'inertie (section 4.0); le développement de l'appareil d'essai de conformité de transport tactique et les étapes suivies pour le modifier (section 5.0) et la représentation du mannequin (section 6.0). La majeure partie du travail consistait en des tâches de développement et de fabrication et ne nécessitait aucune analyse de données, autre que pour établir la justesse et la précision des instruments.

Le présent rapport traite seulement de la partie A du contrat, qui comprend cinq sous-parties. La partie B consiste à modifier les manuels techniques en tenant compte des mises à niveau indiquées dans le présent rapport. La partie C du contrat est fournie séparément et porte sur l'établissement d'un plan et d'un budget à long terme pour l'élaboration d'un modèle biomécanique dynamique. La partie D a été rédigée pour la réunion des spécialistes HFM de l'OTAN, qui est intitulée Soldier Mobility: Innovations in Load Carriage System Design and Evaluation, et qui a eu lieu du 27 au 29 juin 2000. Une description en est donnée dans le compte rendu technique ORT MP-56 intitulé « La mobilité du combattant : innovations dans la conception et l'évaluation des gilets d'intervention [document en anglais seulement] ».

Executive Summary

The purpose of this contract was to upgrade the equipment and improve the instrumentation in support of research and development into dynamic biomechanical modeling for better LC design and system evaluation, and development of a new STANAG for load carriage and is reported in two phases. The Phase 1 report deals primarily with hardware components needed to develop a dynamic biomechanical model. Each subsection of the study will be described in summary below.

A.1 Fastrak™ Software for Relative Pack-Person Motion

The Fastrak™ is a six-degree of freedom tracking instrument that uses electromagnetic fields to determine the position and orientation of a remote object. Our original set-up had the source mounted on the mannequin and either: 1) one sensor placed in the pack for pack-person motion or 2) four sensors placed in the soldier's kit for kit-person motion. This set-up provided 3D pack-person motion only; however, this set-up did not tell us whether the pack and kit were in-synch with the person. Hence it was necessary to revise the dynamic biomechanical model. The set-up and software development was revised with the addition of a second sensor as a ground reference point. This approach allowed us to determine if the pack and person were in-phase or out-of-phase, and the relative amplitudes of their motions. A physical structure was mounted in the ceiling to hold the sensor. Most of the work, however, dealt with the revision of the software. The new software analysis program can be used for several purposes: a) it can examine the frequency content of the pack and person during standardized motions on the LC Simulator, b) it can be used to determine whether a suspension system can be designed to transfer mechanical energy within the gait cycle to assist the person in walking, and c) it can be used to create a better dynamic biomechanical model (DBM) because it can help model the actions of the pack-person interface force requirements.

A.2 Construct Small Strap Force Gauges

The current design for strap force sensors are dog-bone shaped and made out of an aluminium base plate with rosette strain gauges that require a minimum of 6 cm of strap length. These strap force sensors are linear and robust and the design works well for shoulder straps and the waist belt. However, they are not suitable for load-lifter straps and hip stabilizer straps because of length of strap available and the radius of curvature at some locations around the shoulders and hips. The purpose of this phase was to construct and calibrate smaller strap tension sensors to access the difficult-to-measure straps (i.e., load lifters, hip stabilizers). The goal was to develop eight strap gauges that could withstand the same tension ranges (~ 50N to 100N) but be used in tight locations. These sensors were constructed, calibrated and checked for linearity and DC offset. Physical length of the new gauges is 18 mm and they can be sewn into position. Each sensor is now available for use.

A.3 Construction of a Moment of Inertia Platform

One requirement of dynamic biomechanical modeling (DBM) is to know the location of the centre of gravity and the moment of inertia of a pack. Due to the non-uniform nature of a backpack, pinpointing the centre of gravity can be difficult and mathematically calculating the moment of inertia of a non-uniformly shaped and weighted object requires complex equations. A trifilar pendulum provides a relatively simple and quick method of locating the centre of gravity and the moment of inertia of non-homogenous objects. A trifilar pendulum was built which consisted of a round laminated plywood circular plate that was suspended in the horizontal plane by three cables of equal length equidistantly placed from the centre of the plate. When the pendulum is twisted around a vertical axis running through the centre of the plate, it oscillates with a period dependent on the following factors: the length of the cables, the radius of the plate, the mass of the plate, the local force of gravity, and the moment of inertia of the plate. This trifilar pendulum was calibrated and will be used to find the centre of gravity and moment of inertia of backpacks for the dynamic biomechanical model.

A.4 Modify Load Carriage Compliance Tester

The compliance tester was originally developed to assess the stiffness of equipment worn on the torso using quasi-static motion. Movement of the test torso was achieved using a series of hand operated pulleys and cables. This required an operator to attempt to produce a constant rate of displacement that introduced some variability in the methodology and confined testing to quasi-static conditions. The purpose for the revised LC Compliance tester design modification was to support the development of a biomechanical model of human load carriage. The device will furnish input values for the dynamic stiffness variables during initial modelling stages. At later stages of the model development, the apparatus can be used to validate the model by comparing the model predicted stiffness responses to a different range of motion profiles. Only 2D changes were made to the LC Compliance tester at this time with the 3D function to be completed later. These changes to the automated programmable motion control system create a number of functions not possible with the previous system. These functions include: 1) highly repeatable motion profiles independent of the operator; 2) determination of the system stiffness under dynamic conditions; 3) provision for quantitative validation of models of load carriage devices; 4) determination of the frequency response of LC suspension systems; and 5) creation of an automated test cell requiring minimal operator expertise and low cost for possible sale to support other countries' modeling efforts.

A.5 Create Full Body Mapping of Mannequin

Our previous work with static biomechanical modelling yielded relatively good results if the pack was kept simple (i.e. shoulder straps and initial waist belt designs). However, as more pack elements were added (i.e. load lifter straps, hip stabilizers etc) the models were less effective, primarily because of the difficulty in properly modeling the pack-person interface forces. The purpose of this equipment upgrade was to allow a pressure measurement system to be used as an input to the dynamic biomechanical model.

This was accomplished in two ways: 1) write new software to allow direct access to the raw data from the TeKScan™ thus creating the potential to extract specific contact force histories from Tekscan™ and 2) to develop the ability to determine normal force vectors and locate them in space on the body by conducting a total body mapping of the 50^{th} percentile male mannequin. For the first objective, a combination of MatLab (a numerical computation and data visualization program) and Microsoft Excel macros was written. This software-based approach was developed to manipulate the files into the appropriate formats compatible with MSC Visual Nastran™ 4D and 2D Working Model. A full body mapping of the 50^{th} percentile mannequin is necessary to locate the sensels in 3D space, and it will allow the calculation of the normal reaction force. The LC mannequin was scanned so that the full body mapping files are now accessible by Visual Nastran 4D for validation of the waist belt model. The resolution of this scan was 2mm.

Sommaire

Le contrat visait à mettre à niveau l'équipement et à améliorer les instruments, qui serviront à la R et D sur la modélisation biomécanique dynamique en vue d'améliorer la conception et l'évaluation des systèmes de transport de charge, et à élaborer un nouveau STANAG sur le transport de charge. Il comporte deux phases. Le rapport sur la phase 1 porte principalement sur le matériel nécessaire à l'élaboration d'un modèle biomécanique dynamique. Une brève description de chaque sous-section de l'étude est donnée ci-dessous.

A.1 Logiciel Fastrak[MC] pour mesurer le mouvement relatif entre un sac à dos et une personne

Fastrak[MC] est un instrument de localisation à six degrés de liberté qui utilise des champs électromagnétiques pour déterminer la position et l'orientation d'un objet éloigné. Dans la configuration originale, la source était installée sur le mannequin et 1) un capteur était placé dans le sac à dos pour détecter le mouvement sac/personne ou 2) quatre capteurs étaient placés dans le fourbi du soldat pour détecter le mouvement fourbi/personne. Cette configuration permettait de connaître seulement le mouvement sac à dos/personne en trois dimensions; toutefois, elle ne permettait pas de savoir si le mouvement du sac et du fourbi était synchronisé avec celui de la personne. Donc, il a fallu modifier le modèle biomécanique dynamique. La configuration et le logiciel ont été modifiés en tenant compte de l'ajout d'un deuxième capteur comme point de référence au sol. Cette méthode a permis de déterminer si les mouvements du sac à dos et de la personne étaient en phase ou déphasés et de connaître l'amplitude relative de ces mouvements. Une structure a été posée au plafond pour contenir le capteur. La majeure partie du travail a été consacrée à la modification du logiciel. Le nouveau logiciel d'analyse peut être utilisé à plusieurs fins, soit a) examiner les fréquences produites par le sac et la personne durant des mouvements normalisés effectués avec le simulateur LC, b) déterminer si un système de suspension capable de transférer l'énergie mécanique au cycle de marche peut être conçu afin de faciliter les déplacements de la personne et c) améliorer le modèle biomécanique dynamique (DBM) en modélisant les forces exercées au niveau de l'interface sac-personne.

A.2 Fabrication de dynamomètres de sangle plus petits

Actuellement, les capteurs de force de sangle sont en forme d'os à chien et consistent en une plaque d'aluminium dotée d'extensomètres en rosette qui nécessitent une sangle d'au moins 6 cm de longueur. Ces capteurs de force de sangle sont linéaires et robustes, et leur conception est bien adaptée aux sangles portées aux épaules et à la taille. Toutefois, ils ne conviennent pas aux sangles de levage de charge et aux sangles de stabilisation aux hanches en raison de la longueur de sangle disponible et du rayon de courbure à certaines parties des épaules et des hanches. Cette phase visait à fabriquer et à étalonner des capteurs de traction de sangle plus petits afin de permettre la mesure sur les sangles difficiles d'accès (c.-à-d. les sangles de levage de charge et de stabilisation aux hanches). L'objectif était de mettre au point huit dynamomètres de sangle qui peuvent

tenir à la même plage de traction (~ 50 N à 100 N) tout en étant utilisés dans des endroits exigus. Une fois les capteurs fabriqués et étalonnés, on a vérifié la linéarité et le décalage c.c. Les nouveaux capteurs mesurent 18 mm de long et peuvent être cousus en place. Tous les capteurs sont maintenant prêts à être utilisés.

A.3 Fabrication d'une plate-forme de moment d'inertie

Le modèle biomécanique dynamique (DBM) exige que l'on connaisse le centre de gravité et le moment d'inertie d'un sac à dos. En raison du caractère asymétrique d'un sac à dos, il est difficile de déterminer avec précision le centre de gravité de ce dernier et, pour calculer le moment d'inertie d'un objet dont la forme et le poids sont inégaux, il faut recourir à des équations complexes. Un pendule trifilaire constitue un moyen relativement simple et rapide pour déterminer le centre de gravité et le moment d'inertie d'objets non homogènes. On en a fabriqué un en utilisant une plaque circulaire en lamellés de contreplaqué et on l'a suspendu sur le plan horizontal en utilisant trois câbles de même longueur placés à distance égale du centre de la plaque. Lorsque le pendule tourne autour d'un axe vertical passant par le centre de la plaque, il oscille selon une période fondée sur les facteurs suivants : la longueur des câbles, le rayon de la plaque, la masse de la plaque, la force de gravité locale et le moment d'inertie de la plaque. Le pendule trifilaire a été étalonné et sera utilisé pour déterminer le centre de gravité et le moment d'inertie des sacs à dos aux fins du modèle biomécanique dynamique.

A.4 Modifier l'appareil d'essai de conformité de transport tactique

À l'origine, l'appareil d'essai de conformité a été développé pour évaluer la rigidité de l'équipement porté sur le torse dans des conditions de mouvement quasi-statiques. Le torse d'essai était mû au moyen d'une série de poulies et de câbles manipulés par l'opérateur. Ce dernier devait alors essayer de produire une vitesse de déplacement constante. Cela a eu pour effet de créer une certaine variation dans la méthode et de limiter les essais à des conditions quasi-statiques. Les modifications apportées à l'appareil d'essai de conformité de transport tactique avaient pour but d'appuyer l'élaboration d'un modèle biomécanique de transport de charge par une personne. Durant les premières étapes de la modélisation, l'appareil fournira les valeurs d'entrée pour les variables de rigidité dynamique. Durant des étapes ultérieures, il pourra être utilisé pour valider le modèle en comparant les réponses de rigidité prévues avec différents profils d'amplitude de mouvement. À l'heure actuelle, seules les modifications bidimensionnelles ont été apportées à l'appareil; la fonction tridimensionnelle sera ajoutée plus tard. Les changements apportés au système automatisé programmable de commande des mouvements ont donné accès à des fonctions qui n'existaient pas dans le système précédent, notamment : 1) profils de mouvements très reproductibles, indépendants de l'opérateur, 2) détermination de la rigidité du système dans des conditions dynamiques, 3) validation quantitative de modèles de systèmes de transport de charge, 4) détermination de la réponse en fréquence des systèmes de suspension de transport de charge et 5) création d'une cellule d'essai automatisée peu coûteuse ne nécessitant pas beaucoup de compétences de la part de l'opérateur, qui peut être vendue afin de soutenir les activités de modélisation d'autres pays.

A.5 Créer une représentation intégrale du corps du mannequin

Nos recherches antérieures relatives au modèle biomécanique statique ont donné des résultats relativement bons lorsque le sac à dos était simple (c.-à-d. modèles initiaux avec sangles d'épaule et ceinture). Cependant, avec l'ajout d'éléments supplémentaires au sac (sangles de levage de charge, sangles de stabilisation aux hanches, etc.), les modèles ont perdu de leur efficacité, principalement en raison de la difficulté à modéliser correctement les forces à l'interface sac-personne. La mise à niveau de l'équipement avait pour but de permettre l'utilisation d'un système de mesure de la pression comme entrée du modèle biomécanique dynamique. À cette fin, les deux modifications suivantes ont été apportées : 1) création d'un nouveau programme pour permettre l'accès direct aux données brutes de l'appareil Tekscan[MC], ce qui permet d'extraire des historiques spécifiques des forces de contact à partir du Tekscan[MC] et 2) création d'une représentation intégrale du corps d'un mannequin représentant le 50^{e} centile de sexe masculin afin de déterminer les vecteurs de force normaux et de les localiser sur le corps. Pour atteindre le premier objectif, des macros ont été écrites en MatLab (programme de calcul numérique et de visualisation de données) et en Excel, de Microsoft. Cette méthode fondée sur logiciel a été élaborée afin de convertir les fichiers aux formats appropriés, compatibles avec le modèle de travail 2D et 4D MSC Visual Nastran[MC]. Une représentation intégrale du corps du mannequin mâle du 50^{e} centile est nécessaire pour localiser les capteurs à cellules dans un espace tridimensionnel afin de permettre le calcul de la force de réaction normale. Le balayage du mannequin utilisé pour le transport des charges a été effectué, et les fichiers de mappage du corps entier sont maintenant accessibles au moyen de Visual Nastran 4D pour fins de validation du modèle de ceinture. La résolution du balayage est de 2 mm.

Table of Contents

List of Figures

List of Tables

1.0 Introduction

The work on the Dynamic Biomechanical Model (DBM) has been underway after the duties related to the NATO Load Carriage Workshop were completed. One of the outcomes from the NATO HFM Specialist Meeting entitled "Soldier Mobility: Innovations in Load Carriage System Design and Evaluation" held on 27-29 June 2000, was to work toward the development of a NATO STANAG based on the new knowledge developed by various countries involved in research related to load carriage. The contribution Canada can make toward this aim is the development of the minimal biomechanical human tolerance limits based on such variables as shoulder reaction forces, lumbar reaction forces and pressure tolerance limits. One method to acquire these data is to develop a dynamic biomechanical model that can provide direct input of load control and load transfer conditions from soldier trials with different systems. Eventually this biomechanical model could be used in conjunction with a portable measurement system to provide on-line feedback about these variables to identify the magnitudes at which local muscular fatigue or pain occurs that can affect operational effectiveness. Using this modified equipment and a DBM design tool, there is also the potential to enhance our understanding and thus optimization of the transfer of mechanical energy between the pack and person in the design of new systems thus creating "a smart LC system".

1.1 Purpose

The purpose of this part of the study was to upgrade the equipment and instrumentation in support of research and development into dynamic biomechanical modeling for better design and LC system evaluation, and development of a new STANAG for load carriage. Only the equipment prepared in Phase 1 Part A of this multi-phase study will be described in this report, namely:

1.0 Introduction
1.0 Fastrak™ software for relative pack-person motion
2.0 Construct small strap force gauges
3.0 Construction of a moment of inertia platform
4.0 Modify Load Carriage compliance tester
5.0 Create full body mapping of mannequin.

2.0 Fastrak™ software for relative pack-person motion

2.1 Background

In the previous research and development phases to develop the LC Simulator (Stevenson et al., 1995; 1997), a four channel electromagnetic sensing system was used to detect relative pack-person motion. The FASTRAK™, by Polhemus Navigation Incorporated, Colchester, Vermont, USA is a six-degree of freedom tracking instrument that uses electromagnetic fields to determine the position and orientation of a remote object. The system consists of three components: a systems electronic unit (SEU), a source, and up to four sensors. The source generates a low frequency electromagnetic field that is detected by the sensors. The SEU calculates the three dimensional position and orientation of the sensor in this field relative to the source. This is accomplished by interpreting the interaction of the electromagnetic fields between three sets of orthogonal coils contained in both the source and the sensor (An et al., 1988; Day et al., 1998; Polhemus, 1995). The sensors can be detected by the source up to a maximum separation distance of 305 cm, but it is recommended that all testing occur within 76 cm of the source. The specifications state that any metal within the 76 cm envelope may cause inaccurate position and orientation data, but calibration performed by direct comparison of Fastrak™ positional data with data collected from an opto-electric positional recording system (Optotrak™ by Northern Digital Incorporated) with high precision (RMS error <0.01 mm) provided an RMS error for Fastrak™ data of 0.65 mm (Stevenson et al., 1995). Figure 2-1 is a picture of the source and a sensor.

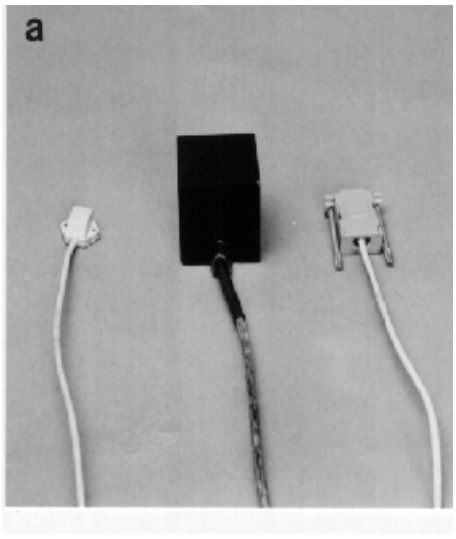

Figure 2-1. Fastrak™ sensor (left) and source (centre). Data are taken via the RS232 port connection (right) to a portable computer.

In the APLCS (Advanced Personal Load Carriage System) project, the FASTRAK™ source was affixed with nylon screws to the underside of the left arm of the mannequin so that the Z axes was superimposed on the mannequin's longitudinal axis. This allowed the source to represent the orientation of the body axis as the global reference for the pack motion. The source was oriented such that the X axis corresponded to the sagittal plane, the Y axis corresponded to the transverse plane, and the Z axis corresponded to the frontal plane. In other words, the front/back (anterior/posterior) motions were recorded by the ± X direction, side-to-side (medial/lateral) motions by the ± Y direction and up-down (superior/inferior) motions were represented by ± Z direction. Pack resultant motion was calculated for pack-person relative displacement.

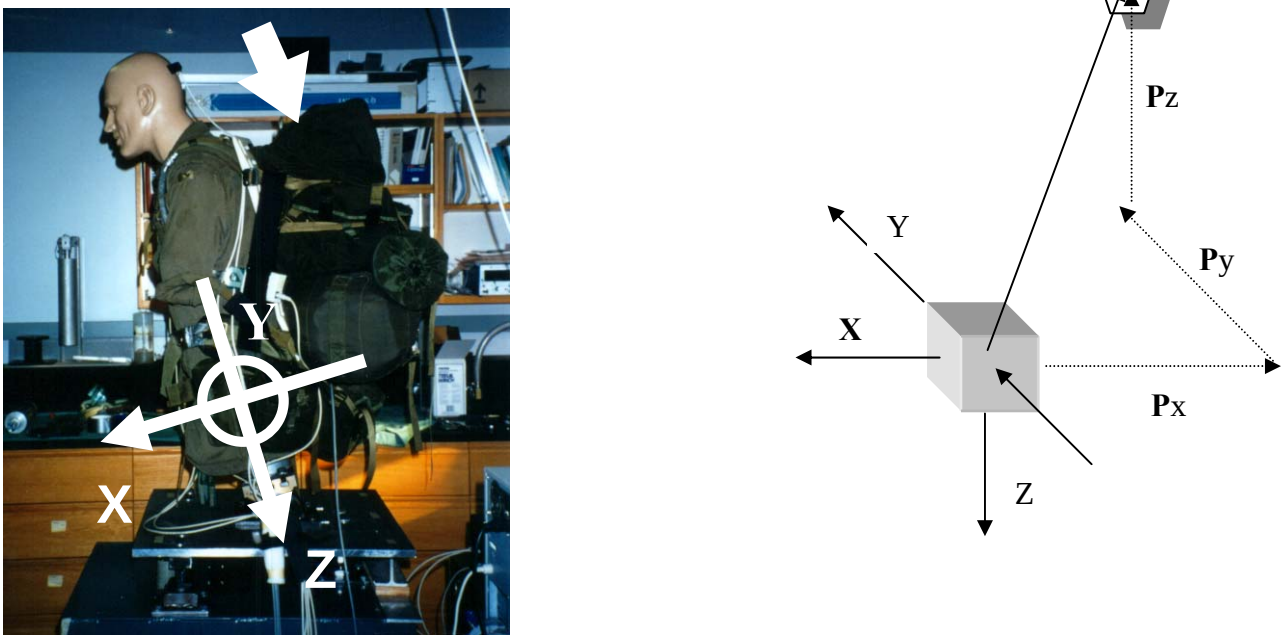

Figure 2-2 Original set-up for assessment of relative motion for Fastrak™ system.

For typical pack-based protocol on the LC Simulator, the source is mounted securely to the left arm with angled plexiglass and plastic screws. A Fastrak™ sensor would be placed securely into the superior polystyrene surface of the LC System payload in order to acquire displacement data for the payload with respect to the source. Data would be collected for 10 seconds at 55 Hz on 300 second intervals over a 15 minute test duration. Coordinate transformation was applied to translate from the superior payload sensor location to the loaded pack centre of gravity to estimate resultant displacement vectors between the centre of gravity of the loaded LC system and the mannequin. The typical output from the previous data analysis is shown in Figure 2-3.

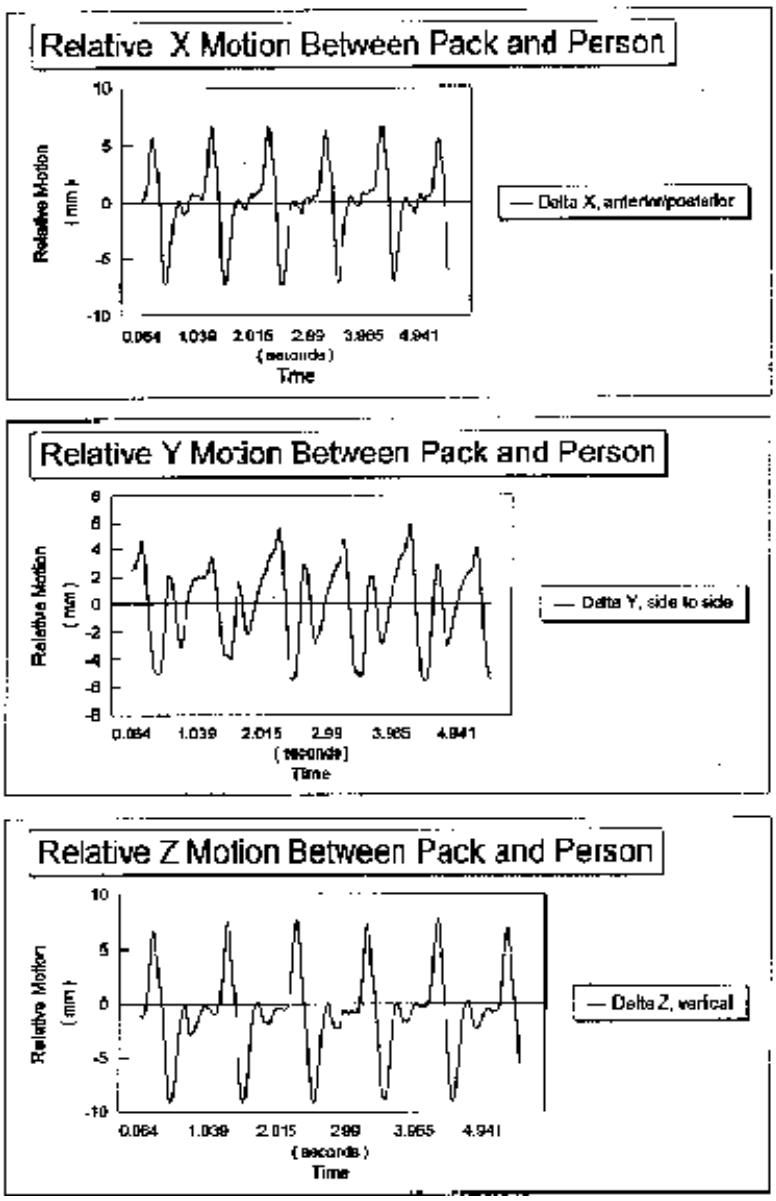

Figure 2-3. A superior LC system (top 10th percentile) would have relative motion values between the pack and person of 1.32 mm in the x direction, 1.06 mm in the y direction and 8.16 mm in the z direction.

Based on the database of load carriage systems tested, the amount of x, z, and r (total relative motion) was related to soldier hip discomfort scores (Bryant et al., 1997). Increased displacement of the LC system, with respect to the soldier, can also decrease agility due to reduced load control. Unrestrained displacement of marching order kit and LC equipment also leads to stability problems and local discomfort due to repeated collisions between the soldier and the pack and other kit items.

2.2 Rationale for Revised Relative Motion Data

Martin et al. (1982) felt that if the load moved independent of the soldier during load carriage, more energy must be used to control the pack and greater fatigue would develop. Therefore, they hypothesized that control of the relative motion between pack and person was important so that load carriage system moved with, rather than oppose the wearer's normal gait pattern. It is this concept that lead Queen's to propose relative pack-person motion that represent a superior top 10% pack (Table 2-1) as the standard of acceptability for future load carriage systems. In other word, pack-person motion that was as small as possible was deemed the best situation for load control and load transfer.

Table 2-1. Pack-Person delta displacement values that represent the 10^{th} , 50^{th} and 90^{th} percentile of seventeen packs from database.

Direction	10^{th} (low) Decile	Mean (50^{th}) Decile	90^{th} (high) Decile
X (mm)	1.32	6.82	12.33
Y (mm)	1.06	3.83	66.60
Z (mm)	7.47	11.32	15.17
R (mm)	8.16	14.06	19.97

Kram in 1991 attempted to explain why Asian people carried loads using compliant springy bamboo or wooden poles on the shoulders (Figure 2-3). At the recent NATO conference, Kram further hypothesized that these springy carrying poles acted like a spring-mass system where the poles should vibrate at 1 Hz if the person is walking at a 3 Hz pace. This would create a natural frequency of vibration equal to the square root of k/m where k is the spring stiffness and m is the mass supported by the spring. Although Kram (1991) was not able to demonstrate his theory of energetics for this system, he felt that compliant suspension systems would allow better energy transfer to take place.

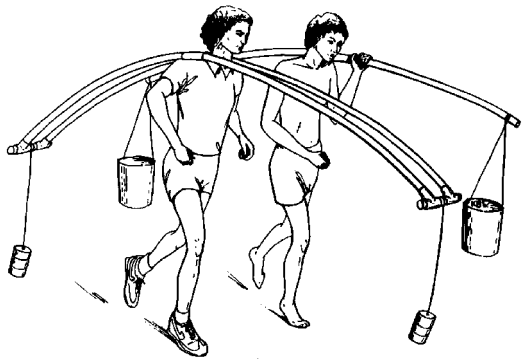

Figure 2-4 The walker causes the poles to vibrate out of phase this each step so there is transfer of energy from the pole to the person (with permission of R. Kram, 2000).

Kram (2000) described the relationship between gravitational potential energy (mgh) and kinetic energy (1/2 mv^2) as an inverted pendulum-like mechanism during walking whereby the interchange saved the body from work to lift and accelerate the center of mass during each step (W_{com}). Based on measuring the metabolic cost of normal walking, most humans appear to recover about 65 % of the energy from step to step, less than the 75% Heglund et al. (1995) found with trained head load carriers. Heglund et al. (1995) found that experienced head load carriers could carry up to 20% of their body mass on their heads with no measurable increase in metabolic energy consumption but Kram (2000) found a linear increase of the metabolic relationship for loads carried at waist level over the same 20% load increase. Both researchers found that recovery of mechanical energy increased with heavier loads but the mechanical work performed on the center of mass plus load did not increase for loads greater than 20% of body mass. Kram (2000) hypothesized that the metabolic cost of walking was determined by three factors: cost of performing external work, cost of generating muscular force to support body weight and cost of swinging the limbs. These costs can change with tasks performed. For example during running, tendons can return as much as 93% of the energy stored in them (Alexander, 1988) thus saving the muscles from the task repeatedly performing work to lift and accelerate the center of mass during each step thus dramatically reduces metabolic cost.

Kram (2000) used these concepts to describe the most appropriate suspension system of load carrying devices similar to using springy bamboo or wooden poles. Using loads on the shoulders, Kram (1991) demonstrated that peak vertical ground reaction force were around 2.5 times body weight but properly tuned carrying pole applied a steady and moderate force with force fluctuations less than 10%, however, there was no metabolic energy savings with springy poles. Kram challenged designers to incorporate compliant suspension systems into load carrying systems used by soldiers and measure the impact of this change.

The concept of a compliant suspension system was part of the impetus to develop the lateral rods in the Clothe the Soldier (CTS) system (Reid et al., 2000). Based on the expert opinion of designer Bill Ostrum from Ostrum Outdoors, he recognized that the rods "worked with" the trekker and seemed to even out the energy requirements. We could not evaluate this potential at Queen's because we did not have the appropriate protocol or software to determine the natural frequency of the pack and person. However, Queen's researchers were able to show that rods under tension could change the required extensor force by the erector spinae and shift some of the force requirements from the shoulders to the waist.

2.3 Purpose of the Fastrak™ Software

This is a new software analysis program which can be used for several purposes: a) it can examine the frequency content of the pack and person during standardized motions on the LC Simulator, b) it can be used to determine whether a suspension system can be designed to transfer mechanical energy within the gait cycle to assist the person in

walking, and c) it can be used to create a better dynamic biomechanical model (DBM) as it can help model the actions of the pack-person interface force requirements. The objective was : to further develop the Fastrak® software for the Load Carriage Simulator to provide phase shift and amplitude information about the motion of the pack relative to the mannequin.

2.4 Software Development

One objective was to develop a protocol that did not affect the standardized approach currently used in LC Simulator testing. Hence, we did not wish to remove the Fastrak® source from its location on the mannequin. The solution was to use a second sensor as the stationary laboratory reference point (0,0,0). In this way, the reference (sensor #2) served to reflect the laboratory coordinates while the Fastrak® source on the mannequin measured as the difference between laboratory coordinates and the mannequin movement (source – sensor#2) and Sensor #1 in the pack measures the difference between the mannequin and the pack's centre of gravity (sensor#1). A schematic of this system is attached as Figure 2-5.

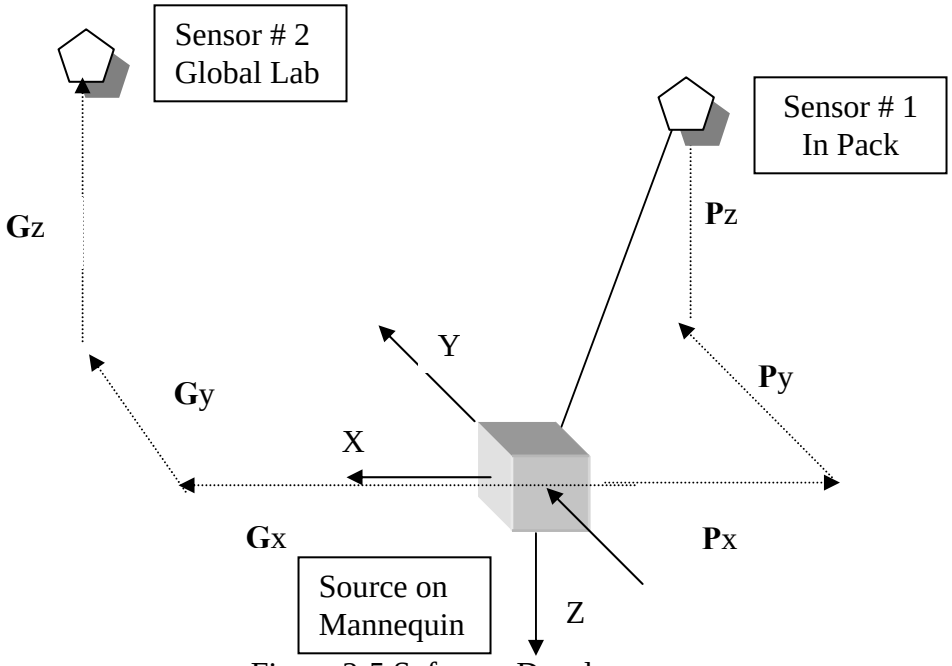

Figure 2-5 Software Development

The relationship of the source (mannequin motion) to sensor #1 (pack motion) and to sensor #2 (global reference). The relative displacement volumes are small and there is no metal interference in the acquisition area.

The global reference sensor is mounted approximately 30 cm below ceiling height on a Plexiglas rod with plastic screws. The source remains on the mannequin's arm and sensor #1 remains in the pack with the coordinates projected mathematically to

the pack centre of gravity. The protocol for data collection remains unchanged in regard to data acquisition. However, there is now additional output from the two sensors into a data acquisition program. The main changes are reflected in the output and analysis programs.

The input program has been changed in the following ways : 1) it now allows multiple trial sets to be gathered without reentry, 2) it retains input information from set to set to allow easier editing, 3) it can collect for a variable number of sensors (1 to 4), and 4) the output file header has been revised to provide additional information – number of sensors and collection frequency in Hz.

The output program consists of two parts: a graphic representation of the data and an ASCII printout (readable by Excel) of frequency-based data. The graphs have been parceled into x, y, and z sheets with (a) as displacement data (in mm), (b) as frequency (in Hz), and (c) as a correlogram of phase shift between the global and pack information. Important information such as ranges, and principal frequencies are also recorded. The peak values for displacement (a) are calculated by identifying the peak amplitudes for each ten second interval and averaging them. The frequency spectrum (b) for each coordinate and trial is calculated from a fast fourier transform (FFT) algorithm using 512 samples (approx 9.3 sec) and providing amplitude and phase values for 128 frequency values from 0.1 to about 13 Hz. The printout is scaled to the highest values of amplitude within each trial with this dominant frequency reported on the left side of the graph as the maximal frequency of the signals for global and pack sensors. The EXCEL printout file captures both the FFT and phase angle as sine/cosine angle information that is needed to return the signal to the time domain. These data will be needed for biomechanical modeling once the response characteristics of the signal are captured in the biomechanical model connection points. The final data display (c) is a correlogram representing a cross-correlation analysis between the global signal and the pack signal. To create this graph, the global signal is held constant in time and the pack displacement signal is shifted to the right by one time step. Then, the root mean square values are calculated and recorded. This process is repeated for a total of 1.2 seconds in order to see where the amplitudes are largest, a point that reflects the phase shift in seconds between the two signals. To avoid jitter at the beginning of the trial, this data collection routine is started after a 30 second delay in sampling. Maximal data are reported in terms of frequency of delay in radians and time of delay in seconds.

Figures 2-6, 2-7, and 2-8 represent the x (anterior/posterior), y (side/side) and z (up/down) data from this program. In the Figures 2.6a, 2.7a and 2.8a, it is possible to see the global displacement data with the amplitudes varying from 24.06 mm, 22.48 mm and 47.31 mm for x, y and z displacement respectively. This makes sense given the LC Simulator input function for gait. The smaller signal on each of the designated graphs represents the motion of the pack, an amount that is approximately 10% of the LC Simulator forcing function. The CTS backpack was superior to most packs in the database at 1.32mm, 0.84 mm and 0.52 mm for pack-person relative motions in x, y, and z planes (Reid et al., 1999). This results mean that the pack suspension system is

acting as a large damper of gait motion thus absorbing much of the original motion so that the pack sensor is only receiving a small percentage of the original displacement amplitudes. It can also be noted in the x and z displacement graphs that the timing of the pack's peak displacements are not in-phase with the mannequin's forcing function.

In Figures 2-6b, 2-7b, and 2-8b, the frequency content of the signal is shown. In all data sets, the maximal frequency is 1.82 Hz. This is the frequency of the forcing function of the LC Simulator for this trial thus providing a validation of the data calculations. This frequency would be expected to dominate. There are small harmonic frequencies shown at 3.6 Hz and 5.5 Hz, a factor that demonstrated a rhythmical nature of the forcing function. Noise in the signals range from 2% to 20% of signal strength. The raw displacement data (a) shows this noise between data points as well. Some of this noise can be removed with better tuning of the forcing function. Another reason for this noise was minor vibration of the global reference sensor that was not isolated from the floor during this sample trial. Lastly, the Fastrak™ raw data signals were not filtered for high frequency noise. With improvements in tuning and isolation, this noise will be reduced to less than 5%. The noise does not interfere with a clear understanding of the signal.

In Figures 2-6c, 2-7c, and 2-8c, the correlogram is being used to show the phase shift or lag between the mannequin's motion to the pack's motion. In the x (forward/backward) and z (up/down) directions, the pack is out of phase with the LC Simulator by 3.02 and 3.44 radians (173º and 197º) respectively. This is also represented by a delay of .29 seconds and .35 seconds respectively. As the conversion of the LC Simulator motion from 1.82 Hz to one cycle period is 0.55 seconds, this represents a complete out-of-phase motion of the pack. The y displacement (side to side) motion is almost in phase with the LC Simulator function as its motion is maximized at 0.66 radians (or 37.8º) of phase shift that can also be described as a time lag of .55 seconds. Without further data, it is not possible to interpret the importance of these findings. However, it is speculated that a particular out-of-phase pattern will be best for transfer of mechanical energy from the pack to the person as speculated by Kram (2000). We plan to study this relationship in the near future.

Figure 2-6. Relative X motion between pack and person: a) x displacement; b) x FFT spectrum and c) x phase shift.

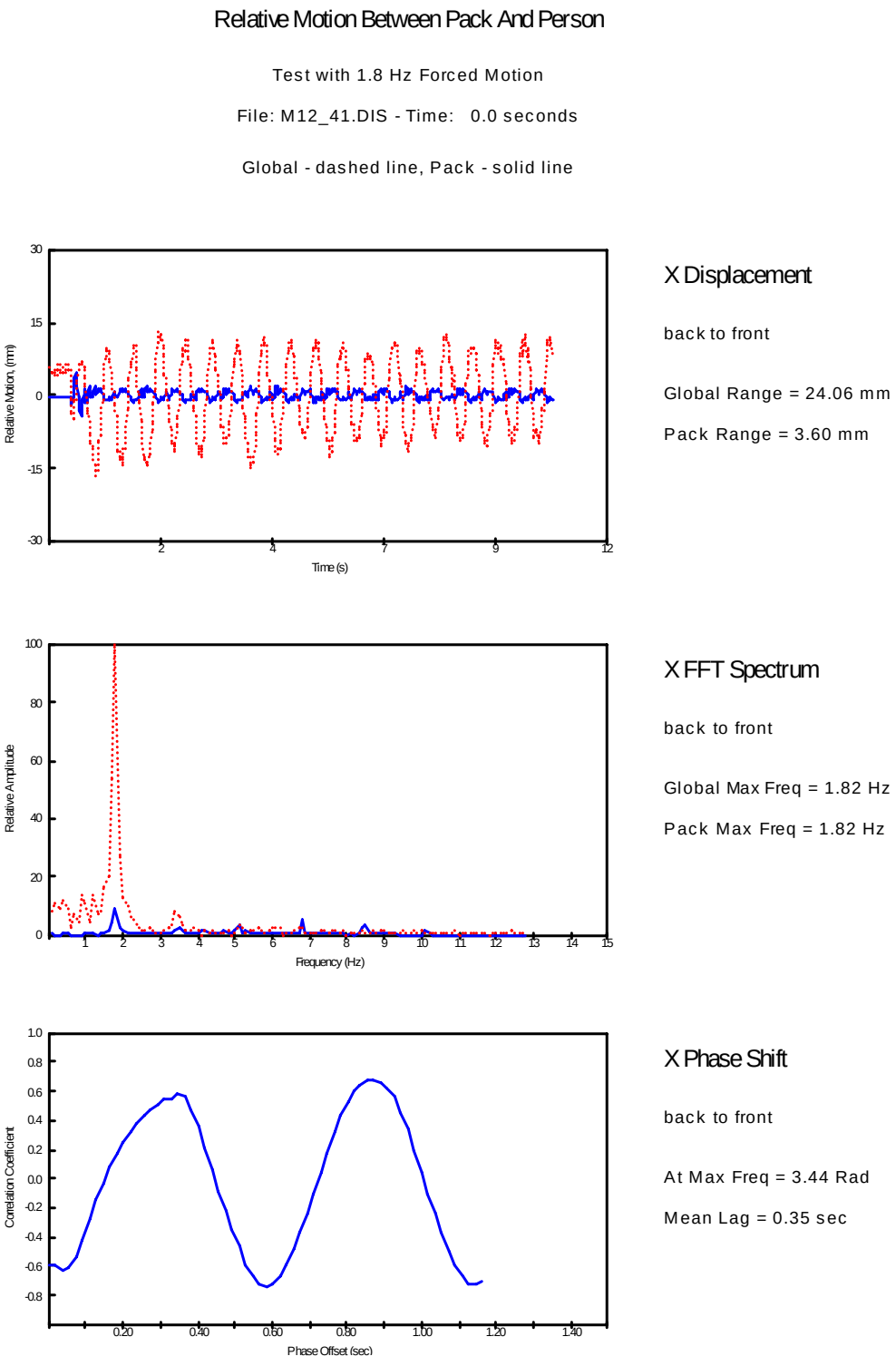

Figure 2-7. Relative Y motion between pack and person: a) y displacement; b) y FFT spectrum and c) y phase shift.

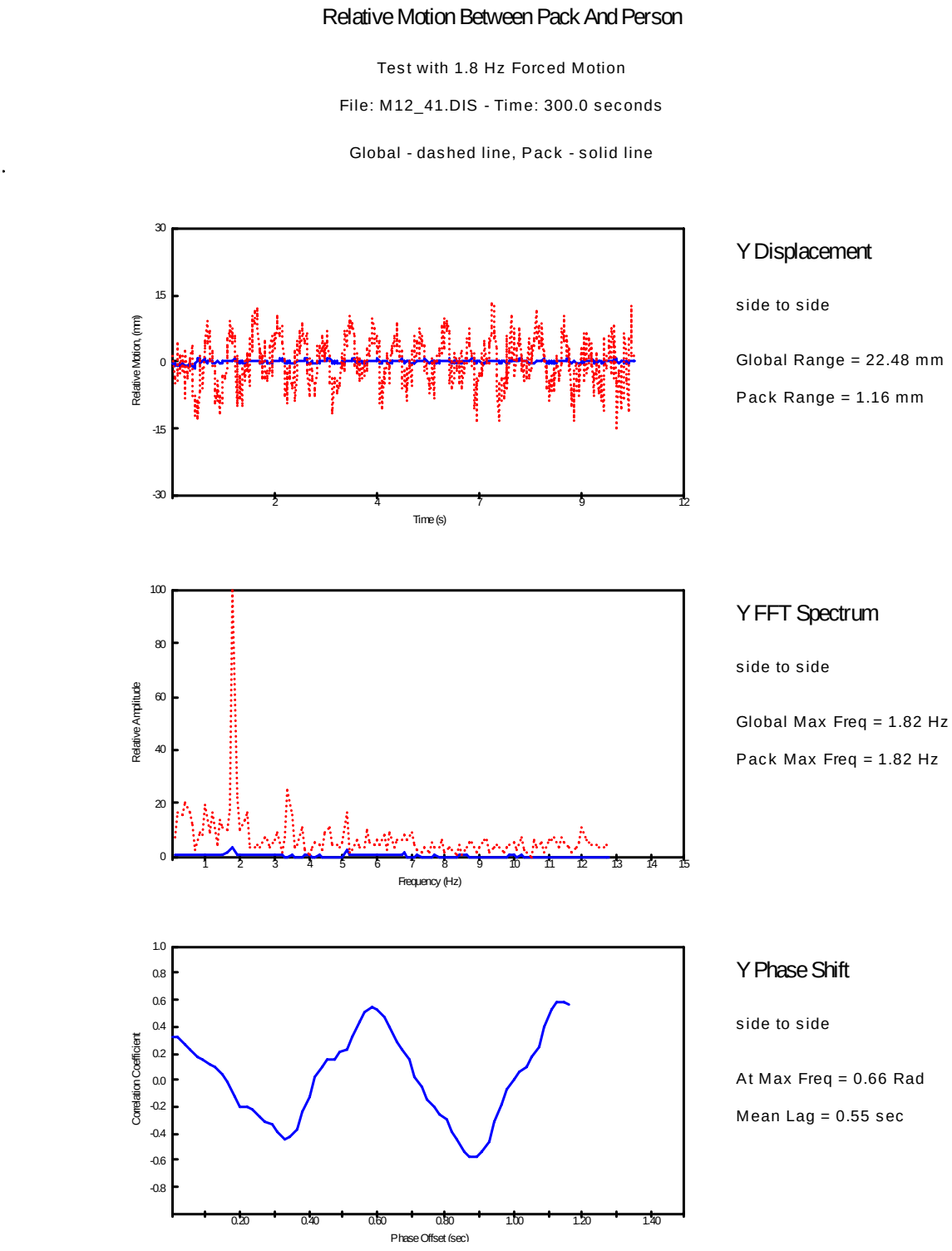

Figure 2-8. Relative Z motion between pack and person: a) z displacement; b) z FFT spectrum and c) z phase shift.

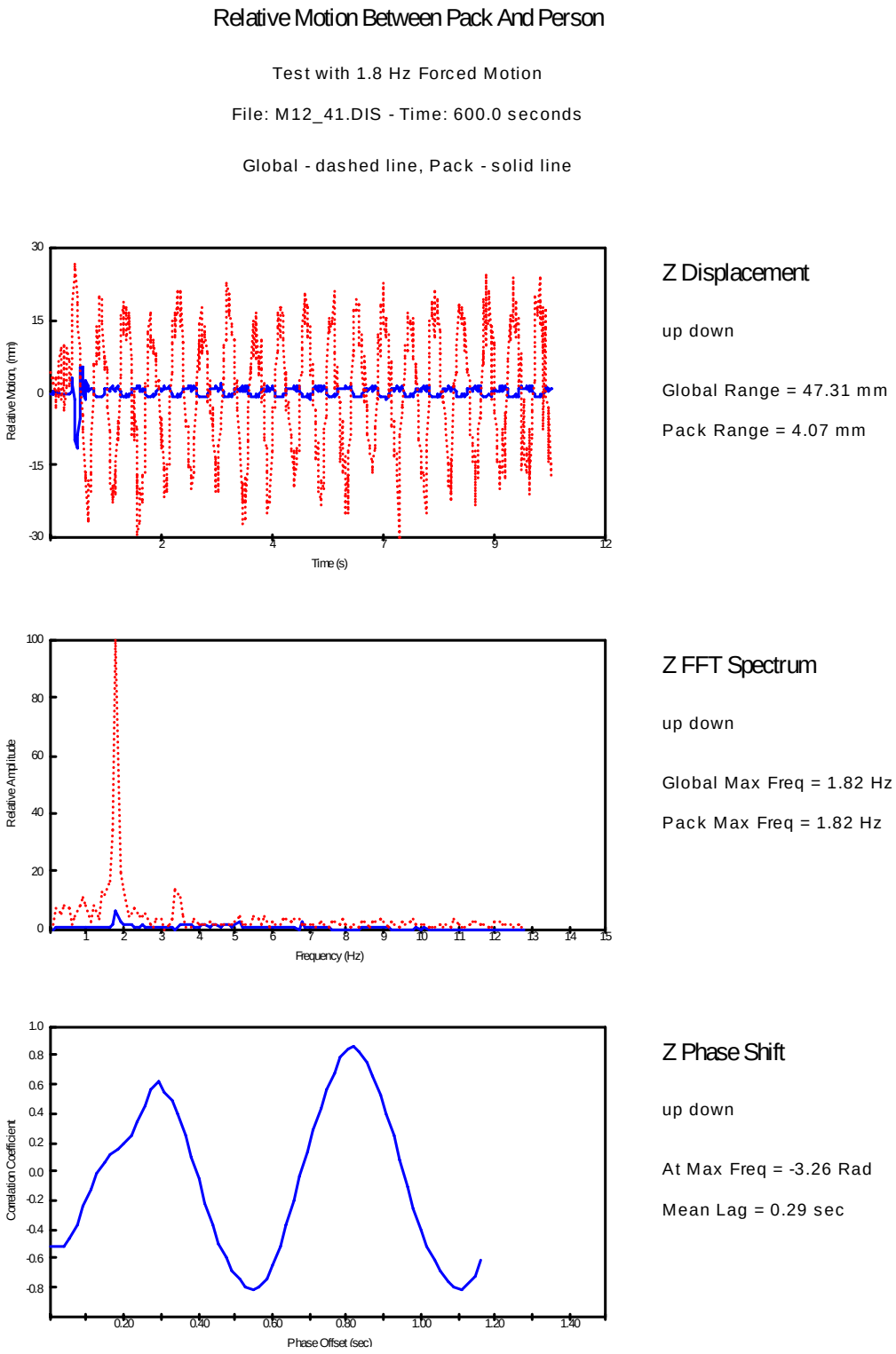

2.5 Uses of Software

One immediate use of the software is with the development of the new DBM model. The resultant motion of the pack is required in order to model the constraints between the two moving systems. The software modification will also allow us to characterize the interface more accurately so that more accurate modelling routines can be developed.

A second use is to determine if there are differences between packs in terms of the mechanical transfer of energy within the suspension system. In Kram's (2000) hypothesis, he suggested that a natural frequency of vibration of a pack is equal to the square root of k/m where k is the spring stiffness and m is the mass supported by the spring. He felt that a pack suspension system could be tuned to apply a steady force with moderate force fluctuations and challenged designers to incorporate compliant suspension systems into load carrying systems and measure the impact of this change.

A third use is to design a dynamic suspension system where the suspension system of the pack can be tuned to create a natural frequency for marching orders. It would be important to also have soldier trials to determine whether there is a net savings of metabolic costs and whether the soldier can "feel" that the pack is now costing less energy. This analysis would be useful to determine the cost-effectiveness of active suspension systems.

3.0 Construction of Small Strap Force Gauges

3.1 Introduction

The current design for strap force sensors is a dog-bone made out of a T6061 aluminium base plate (t=1.25mm, L=39 mm) with two ninety degree "T" rosette strain gauges (Measurements Group Inc. M-M: EA-13-125TG-350) mounted in a full Wheatstone bridge configuration.(Figure 3-1). A stress relief was used to prevent the strain gauges from being torn from their cables. Straight pins are used to suspend the gauge and unload the underlying strap causing all load to be directed through the gauge. These strap force sensors were linear and robust but the hook and pin attachments required a minimum of 6 cm of strap length. This design worked well for the shoulder straps and waist belt. However, it was not suitable for load-lifter straps and hip stabilizer straps because of length of strap available and the radius of curvature at some locations around the shoulders and hips.

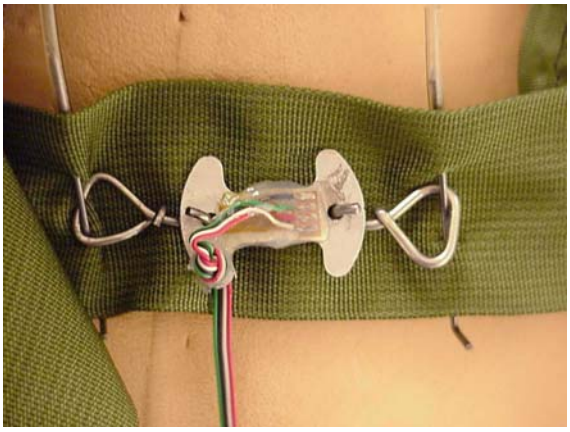

Figure 3-1. Sample "dog-bone" strap sensor used in previous contracts for shoulder straps and waist belts.

3.2 Purpose

The purpose of this work plan was to construct and calibrate smaller strap tension sensors to access the difficult-to-measure straps (i.e., load lifters, hip stabilizers). The goal was to develop eight strap gauges that could withstand the same tension ranges (~ 50N to 100N) but be used in tight locations.

3.3 Methods

A series of aluminium blanks were slit (not sheared) from 1.568 mm thick T6061 Aluminium sheet. Each of these was 18 by 6.5 mm in size. Mechanical designer, Mr. Gerry Saunders from the Human Mobility Research Centre (HMRC) machined the

backing plate shapes, drilled attachment holes at each end of the blanks and cleaned the metal in preparation for gauge mounting. Two ninety degree "T" rosette strain gauges (Measurements Group Inc. M-M: EA-13-062TT-350) were mounted in a full Wheatstone bridge configuration on each blank. A transparent protective coating (M-Coat A, Measurements Group Inc.) was used over the entire surface to water proof the transducer. Physical length of the new gauges is 18 mm (Figure 3-2).

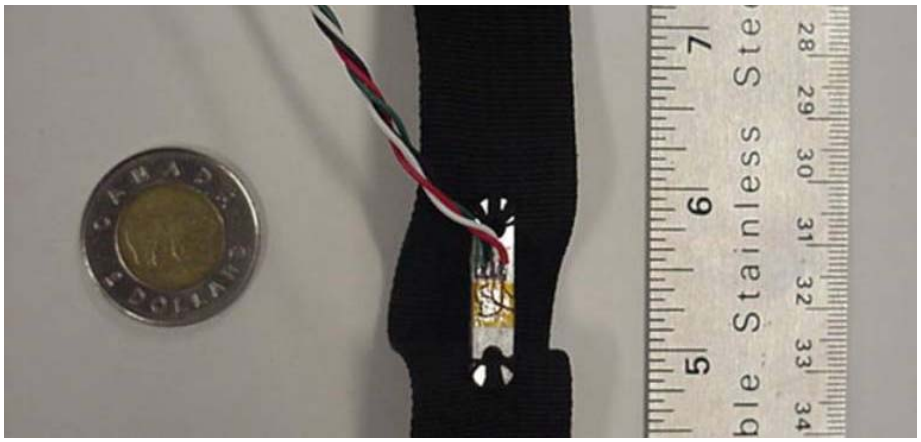

Figure 3-2. Sample of the new miniature strain gauge sewn into a strap.

Nine miniature strap force sensors were made. Each gauge was calibrated with an Instron™ force measurement device under static loads equivalent to the ranges of force used in load carriage conditions. Figure 3-3 depicts the testing set-up.

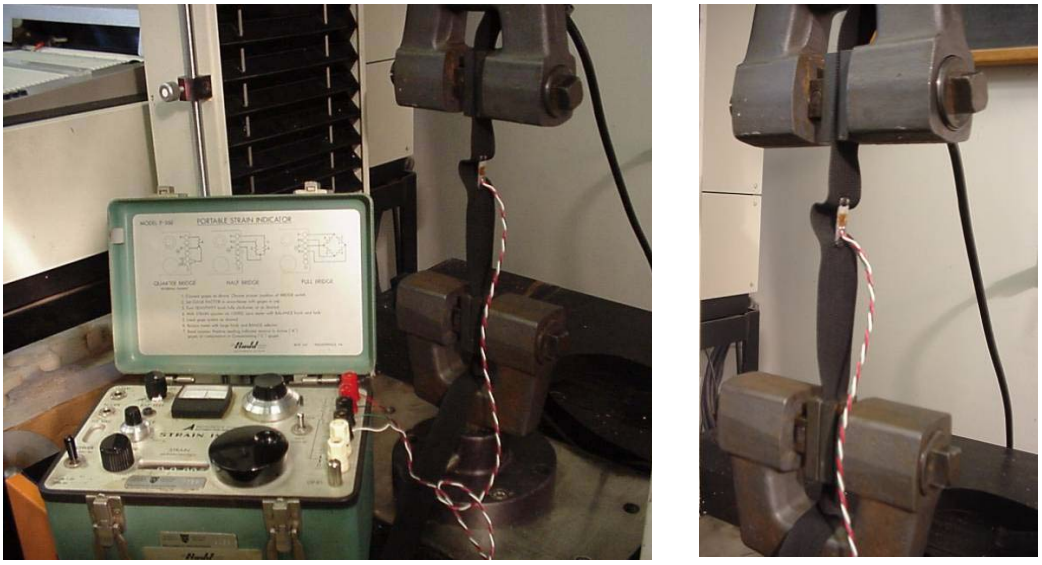

Figure 3-3. Miniature strap force sensor calibration in the Instron. A portable Strain Indicator was used to acquire strain gauge data.

3.4 Results of Calibration

Figure 3-4 depicts a summary of the nine sensors calibrated. The regression R^2 values ranged from 0.9934 to 0.9999 with the correction equations provided in Table 3-1. Only Gauge #7 was less accurate and also had a noisy baseline. The other gauges are highly linear and acceptable for use.

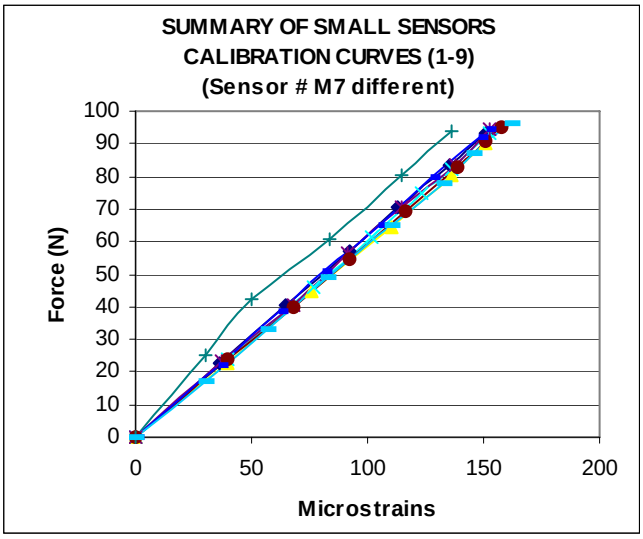

Figure 3-4. Summary of all nine miniature strap force gauges.

Table 3-1. Summary of regression equations for miniature strain gauges.

Gage	Regression Equation	R^2
#1	y= 6.1355x +16.761	0.999
#2	y= 6.1895x + 1.1204	0.9999
#3	y= 5.9705x – 6.2452	0.9997
#4	y= 6.0831x + 3.1883	0.9999
#5	y= 6.1236x – 0.8172	0.9995
#6	y= 6.015 x – 4.8406	0.9998
#7	y= 6.7419x + 37.918	0.9934
#8	y= 6.2446x – 1.0136	0.9999
#9	y= 5.9544x – 4.3228	0.9999

3.5 Discussion and Conclusions

The miniature strap gauges will be suitable for use in most locations. It must be noted however, that these gauges have not satisfied three requirements: they cannot be mounted quickly for field trials, they require the strap to be floating free of underlying material (a difficult task given the nature of the pack design), and they may be more susceptible to damage from bending of the sensor. These design problems will be corrected with the new strap sensor design that is part of the Phase II contract. In addition, in the new sensor design, there would be no need to modify the strap (cut into or sew onto) and it is likely that a sensor could be captured directly by a portable data acquisition system with no requirement for an amplifier (saving power/weight and reducing cost).

In conclusion, and despite these possible limitations mentioned above, these nine strap sensors are only 18mm in length, highly linear, robust and a substantive improvement in size from the previous "dog-bone" sensor design.

4.0. Trifilar Pendulum: Experimental Determination of the Moment of Inertia

4.1 Introduction

One requirement of dynamic biomechanical modeling (DBM) is to know the location of the centre of gravity and the moment of inertia of a pack. It is possible that two packs with the same load and a completely different geometry can have the same centre of gravity and moment of inertia. Due to the non-uniform nature of a backpack, pinpointing the centre of gravity can be difficult. While the packs ideally would be loaded uniformly, it is generally not possible. Attempts can be made to centre the load or have it in the same position relative to the user but the non-rigid, non-uniform shape of the compartments make it impossible.

Mathematically calculating the moment of inertia of a non-uniformly shaped and weighted object requires complex equations. With the proper tools, this process is simplified by physically calculating the centre of gravity and moment of inertia. The most logical method is to construct a trifilar pendulum to make these calculations.

The trifilar pendulum provides a relatively simple and quick method of locating the centre of gravity and the moment of inertia of non-homogenous objects. Its applications go far beyond those of the backpack project. It can be used to measure properties of objects other than backpacks that are worn or carried by soldiers. In addition, the pendulum is large and stable enough to measure centre of gravity and moment of inertia of the human body in any position.

4.2 Theoretical Basis

According to Webster's Dictionary, moment of inertia is 'the ratio of the torque applied to a rigid body free to rotate about a given axis to the angular acceleration thus produced, about that axis and equal to the sum of the products of each element of each mass by the square of its distance from the given axis. Moment of inertia is to rotation as mass is to linear movement. The equation for this is:

$$T=I\alpha$$

The word trifilar consists of 'tri', or three and 'filar', or filaments; a pendulum that is hung with three filaments. It resembles a tire swing with the exception of the insertion points of the top of the filaments. Instead of converging at one point, each filament remains completely vertical with the insertion point directly above the point of insertion on the pendulum plate.

The trifilar pendulum consists of a round plate of a homogenous material, suspended in the horizontal plane by three cables of equal length equidistantly placed from the centre of the plate. When the pendulum is twisted around a vertical axis running through the centre of the plate, it oscillates with a period dependent on the following factors: the length of the cables, the radius of the plate, the mass of the plate, the local force of gravity, and the moment of inertia of the plate [See equation 1, Appendix A].

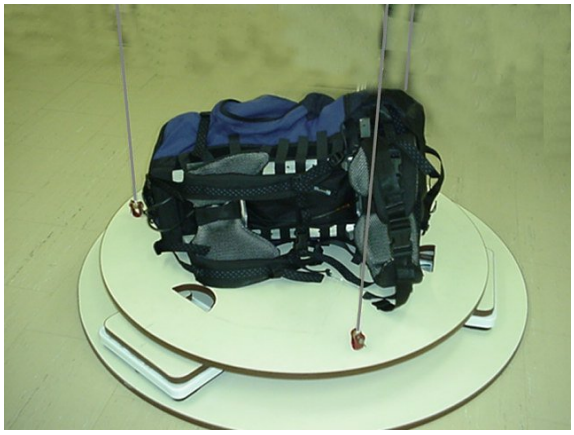

Figure 4-1. Trifilar Pendulum with Pack

When an object is placed on the plate, with its centre of gravity (c of g) above the c of g of the plate, the resultant object/plate combination can be treated as a new pendulum. Since all factors other than mass remain constant, the change in the period of the new pendulum is related to differences in the mass of moments of inertia of the old and new pendulums. The mass can be easily measured and its effect calculated, and the moment of inertia of the object can be determined using a mathematical formula [See equations 2 and 3, Appendix A].

The design is based on two smaller trifilar pendulums that are presently used for 2nd and 3rd year engineering labs at Queen's University. Although these pendulums are too small for measuring backpacks, they represent a proven design that can be scaled up for larger objects. Several modifications were made to increase the stability and safety for measuring properties of humans.

4.3 Strengths and Limitations of Design

There are several strengths of the use of the trifilar pendulum. It requires very simple calculations that can be done on a basic calculator. Once the set-up is installed, it provides quick results and is easy to use. It is relatively inexpensive and upkeep and maintenance is minimal. The equipment is durable and should stand up to years of use. It makes an excellent teaching tool as it has a wide variety of applications and is quite versatile. It is more accurate than many of the other commonly used methods.

There are several limitations to the design as well. The trifilar pendulum has been optimally designed for objects no larger than 0.89m wide, although as long as the entire mass of the object is supported by the plate any length is acceptable. Due to the geometry of the pendulum, the accuracy increases with weight. Therefore objects lighter than 13.6lb have +/-10% error. Human error of the scale reading is variable. Of the mechanical errors involved, one must consider the inherent errors in the scale readout (+/-0.45kg), dimensional tolerances of the plate and irregularities of the plate lamination, accuracy of the filament connections, accuracy of the placement of the scales, horizontal movement of the plate during rotation, and shifting of the load during testing. Non-mechanical errors attributed to the operators include inaccurate scale reading, errors in timing and complete rotation determination, inadvertent horizontal movement and the positioning for the angle of rotation of the plate.

4.4 Design Requirements

Several design requirements had to be considered, they are as follows:

1. Accurate and precise results

The current methods used for finding the moments of inertia of packs require a great deal of guesswork and complex calculations. The trifilar pendulum design provides more mathematically accurate results and has a high level of repeatability.

2. Location (requires a high ceiling for mounting)

Due to the long length of the filaments, installation location was important. Shortening of the filaments due to height restraints would change the properties of the pendulum. The importance of a non-permanent assembly was also important, as the apparatus is located in a classroom. The design allowed for the top cable attachments to be permanently fixed to the ceiling while the pendulum plate and lower plate could be easily moved. The cables can then be hooked up onto the ceiling out of the way as the rest of the assembly is stored in a closet until it is needed.

3. Wide range of applications/different objects

The pendulum was to have more applications than just use with backpacks. The size should be optimal for use with a variety of objects. The size required for packs was used as the main factor, but consideration was given for larger and slightly smaller objects as well. The pendulum can be scaled down if needed for smaller objects.
The maximum weight allowable for objects is 163.6kg.

4. Ease of use

Ease of use was a key issue as the Queen's pendulum is mounted in a classroom. Ease of use also encompasses ease of maintenance and durability. Modifications to the initial design were made to make the attachment of the plate to the filaments easier. With heavier objects resting on the plate, it was difficult to lift the plate to attach the filaments after finding the centre of gravity of the object. A method to raise and lower the plate without unhooking the filaments was designed. The pendulum can be easily used by one or two people.

5. Relative low cost

Relative low cost was important, though not a limiting factor. The simplicity of the pendulum theory allowed for this consideration to be met easily.

6. Safety

The safety of use is an important factor as the pendulum was to be used for finding inertial properties of humans as well as inanimate objects. Several modifications were made from the original design to increase the degree of safety. The addition of a spindle bearing assembly in the centre of the pendulum plate limited the plate's horizontal movement and assisted with smooth rotation. Error effects of this spindle assembly have not yet been determined.

4.5 Final Design Parts List

Details of the final design are provided in the Parts List (Table 4-1). The explanation that follows will comprise the final design.

Table 4-1 - Parts List

Quantity	Name	Description	Material
1	Ceiling Template	Square or circle approx. dia/width 40"	Plywood or similar 3/4"
4	Ceiling Template Fasteners	According to ceiling material	Steel
1	Rotating Plate	Circle dia. 40", 6 holes drilled equidistant - dia. 35", mass=26lb	Fir GIS Plywood 3/4"
1	Lower Plate	Circle dia. 45"	Fir GIS Plywood 3/4"
3	3/16" Steel Cable	3/32" dia., 135" effective length	Stainless Steel Cable
6	Wire Crimpers	3/32" cable size	Steel/Aluminum
6	Clevis	Plain Stem Yoke End Clevis dia 1/2", length 2-1/2"	Steel (painted)
6	Clevis Pin	1/2" dia, 1-1/4" effective length	Stainless Steel
6	Clevis Pin Bushing	1/2" I.D, 3/4" O.D., 9/16" length	Brass
6	Cotter Pin	5/32" dia, 1-1/2" length	Stainless Steel
9	Washer	1/2" Screw Size (9/16" I.D., 1-3/8" O.D.)	Zinc Plated Steel
1	Centre Post	Total length 3”, 2” dia flange, ¼” thick, machined to 0.6693" dia, 2-3/4" length,	Steel
2	Fasteners for Centre Post	Woodscrew, ¾” length	Steel
1	Centre Socket	1.6535" I.D., 1.9035 O.D., 2-1/4" height	Steel
1	Center Socket Flange	3-1/2" dia., 1/4" thickness	Steel
1	Bearing	Needle roller bearing with flanges, without inner ring SKF RNAO17x25x13	StSteel
1	Bearing	Maintenance-Free Spherical Plain Bearing SKF GE25C	StSteel
5	Fasteners for Socket	Woodscrew, ¾” length	Steel
2	Pegs/Rollers	1/2" dia, 3" length	Steel
3	Head Swivel Screws	9/32" dia, 2" length, Techni-Tool #81-10	Steel
3	Threaded Inserts	1/2" I.D., 3/4" length	Steel
3	Bathroom Scales	Danze 63-8083-4 (+/-1lb)	
	Laser Centering Device (optional)		

4.6 Validation Testing to Find Centre of Gravity

For the trifilar pendulum to yield the correct moment of inertia for an object being tested on the pendulum, it is necessary that the c of g of the object be directly above the c of g of the plate, so the centroid of the object and the plate are in line. If the object is regular, it is easy to calculate the c of g mathematically. However, if the object is not symmetrically shaped, or has an uneven mass distribution, it can be quite difficult to locate the c of g mathematically.
Therefore, a system was required that would:

1. Allow the centre of gravity of an object to be determined easily
2. Aid the operator in centering the object on the plate.

4.6.1 Proposed design being tested

The proposed design consisted of a plywood plate, 0.51m in radius, with three drilled holes at 0.44m from the centre. The holes formed the three vertices of an equilateral triangle. Weigh scales were used for measuring the forces at the three drilled points. These scales were calibrated using known weights and found to have a precision of +/- 0.45kg. Force was transmitted using a ball bearing to ensure that the force was being transmitted at a single point. From statics, it is possible to derive the relationship between the c of g of the object and the vertical force on the three locations by the summation of moments.

4.6.2 Methodology of Testing

The system was calibrated at fifteen distinct locations on the plate. Following the theory underlying the device (that the moment of the c of g is balanced by the moments created by the three forces), only locations (points) inside an imaginary triangle formed by the three points were used. If locations outside the triangle were used, the plate would tip, and the results would be useless.

The weigh scales were zeroed to remove the effect of the weight of the plate. A 13.6kg weight with a known centre of gravity was then placed such that its centre of gravity exactly coincided with one of the fifteen calibration locations. The scales were then read, and the results recorded. The object was then removed, the scales re-zeroed, and the object was placed on the second calibration location. This process was repeated until all fifteen calibration locations had been tested. The entire trial was then repeated two more times.

The raw data (location, measured weights) were then analyzed, using the predictive equations for the X and Y.

4.6.3 Statistical analysis of results

If the c of g finder performed perfectly, there would be a 1:1 correlation between the measured X and Y values, and the calculated X and Y values. There was a high

correlation between the actual position of the object and the calculated c of g from the testing. On the X dimension, linear regression yielded a relationship of 0.98:1 with an r squared value of >0.99. On the Y dimension, linear regression yielded a relationship of 0.99:1 with a r squared value of >0.99. This near linear relationship confirms that the theory relating the weights at the three triangle vertices to the location of the object is correct. This relationship can be observed in Appendix D.

4.6.4 Error Analysis

The error ranged from –3.3 to 2.3 cm on the X dimension, and from –4.8 to 2.8 cm on the Y dimension (fig 8, 9). The magnitude of the error does not appear to be affected by the distance from centre (fig 10, 11). The frequency of the magnitude of the errors appears to follow a normal distribution pattern (fig 8, 9).

The total error (E_T) of the system is calculated with the Pythagorean formula. When each trial was completed separately, the average E_T for the three trials was 1.73, 1.4, and 1.5 cm. Since the errors appear to cluster around zero, (fig 10, 11) it was hypothesized that the error could be reduced by averaging the results.

For each location, the weights at the three vertices were measured three times, once per trial. For each location, therefore, there were three calculated X and three calculated Y values. The X values were averaged to yield a new (average) X value, and the Y values were averaged to yield a new (average) Y value.
The average E_T of the new X, Y pairs was only 0.36 inches (Appendix E).
This result can also be seen on the position vs. error charts, where the average values tend to be more accurate (less error) than the non-averaged values.

The level of accuracy of this device could be of concern for some applications. The average absolute total error is 1.55cm (3.5% of the radius), and the maximum absolute error was 4.83cm (10% of the radius). It appears that the accuracy can be increased significantly by averaging the results of multiple trials. Indeed, averaging three trials yields an averaged absolute error of 0.91cm (down from 1.55cm) which is 2.5% of the radius. With this method, the maximum absolute error drops to 1.78cm (down from 4.83cm) which is 4% of the radius of the plate.
The accuracy of the device should increase as the weight of the object being measured increases due to the precision of the scales. The error is +/- 0.45kg, therefore for a 13.6kg object the error is +/- 3.3%, and for a 45.5kg object the error is +/-1%.

4.7 Validation Testing for the Moment of Inertia

In order to validate the accuracy and precision of the pendulum, a known mass with homogenous weight distribution and an easily calculated center of mass and moment of inertia was chosen as the object. The object was rectangular solid with a mass of 17.1 kg. The object was tested using a modification of the “Backpack Protocol” in the following section, although only one axis was tested due to the shape of the object. Instead of the

usual three repetitions per axis, ten were performed on the single axis to determine whether or not there were order effects. After ten repetitions, the object was removed and the apparatus was reset. The test was repeated for another ten repetitions, reset, and repeated, for a total of three sets of data.
An ANOVA two-factor without replication analysis was run. The p-value between the three sets was 0.83 and the p-value between ordered repetitions was 0.35. A p-values that is greater than 0.05 is considered to show no effect of order of repetitions or sets. No effects were shown.
The mean measured time for 10 rotations was 19.863 s with standard deviation of 0.113. The standard error is 0.02 (Appendix D).

4.7.1 Initial Set-up

A suitable room was chosen to accommodate the pendulum. The length of the cables was calculated precisely and was not changed, as this would have effected the mathematical calculations. The length of cables was the optimal value for the size and weight of the suspended plate.

The ceiling template was affixed to the ceiling with proper fasteners that exceed the load that the pendulum is rated to hold. Care was taken to ensure that the plate was level. Three cables were attached to the ceiling plate with the cotter pins.

4.7.2 Test Protocol

1. Place the bottom plate on the floor below the ceiling plate. Arrange the three scales on the plate with the dials facing out and their rubber feet in the corresponding indents on the plate.
2. Clean the shaft on the underside of the pendulum plate to ensure it is free of dust and debris. Insert it into the socket on the bottom plate. This must be done carefully as the socket contains a bearing.
3. Tare the scales.
4. Attach the cables to the turnbuckles on the pendulum plate. Reposition the bottom plate in order to line up the swivel head screws with their respective indents on the tops of the scales.
5. Adjust the swivel head screws to a uniform height, ensuring that the full weight of the plate is on them. The cables should be slack.
6. Tare the scales.
7. Place the load on the pendulum plate. Position it such that each scale is weighted evenly.
8. Gently lower the swivel head screws until the cables are tensioned and the plate is suspended. If the load shifts, lower the plate and repeat the centering steps.
9. Insert the angle measurement pegs.
10. Rotate the pendulum plate slowly until it is displaced ten degrees.
11. Release the pendulum plate in conjunction with the beginning of timing.
12. Record the time required to complete ten full rotations.
13. Repeat steps 10 through 12 three times and average the final result.
14. Take a digital photo from as close to directly above the pendulum plate as possible.
15. Raise the swivel head screws until the plate is evenly supported on the scales.
16. Reposition the object for calculations about a different axis.
17. Repeat steps 7 through 14.
18. Reposition the object for calculation about the final axis, steps 7 through 14.

4.7.3 Calculations

The governing equation used to calculate the moment of inertia about each axis is:

$$I = \frac{0.2485r^2}{l}\left(mT^2 - m_pT_p^2\right)$$

Where :

$I = \text{mass moment of inertia } (kg \cdot m^2)$

$m = \text{mass of plate/object combination } (kg)$

$T = \text{period of plate/object combination } (s)$

$m_p = \text{mass of plate } (kg)$

$T_p = \text{period of plate } (s)$

$r = \text{effective radius of plate } (m)$

$l = \text{length of filaments } (m)$

Details can be found in Appendices.

4.7.4 Location of the Centre of Gravity of a Backpack

Figure 4-2. To locate the centre of gravity, the photos taken after each pack position are manipulated as seen. The point at which the bisecting lines cross in the centre is the position of the centre of gravity of the pack in that plane.

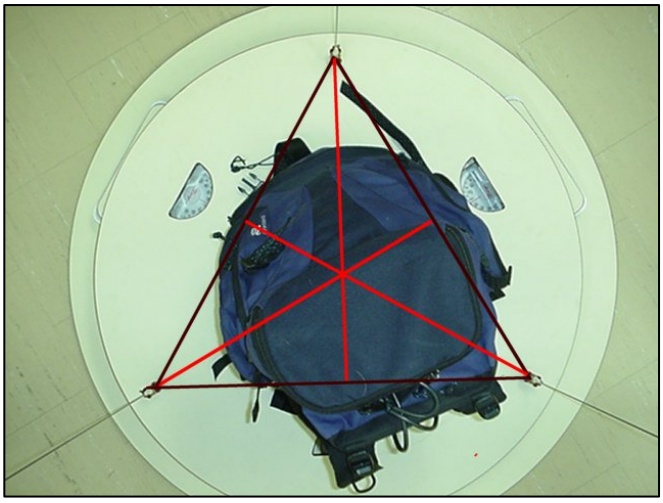

4.7.5 Conclusions

The trifilar pendulum design has proven to be a simple and user friendly apparatus to determine the centre of gravity and moment of inertia of irregularly shaped objects. Most of the design considerations have been met, although the accuracy of the design will be improved with testing of the new model, outlined in the detailed drawings.

5.0 Automation of the Load Carriage Compliance Tester

5.1 Introduction

Immobilisation of the torso has been shown to increase a person's energy expenditure in walking at moderate speeds by about 10%.[1] Energy cost was more than twice that of carrying a 5kg weight about the waist. When applied to load carriage, the upshot is: the greater the resistance to normal body movement, the greater the baseline energy cost for a load carriage system. As well, good torsional compliance is necessary to assure free relative motion between the shoulders and hips during agility activities. The rigidity of a LCS is inversely correlated, $(r^2>0.86)^2$ to a number of performance parameters such as: comfort of the user, a wearer's ability to perform whole body motions, and the ability to perform tasks requiring upper arm/shoulder mobility such as moving ones' arms to the front or overhead.

The compliance tester was originally developed to assess the stiffness of equipment worn on the torso using quasi-static motion. Movement of the test torso was achieved using a series of hand operated pulleys and cables. This required an operator to attempt to produce a constant rate of displacement which introduces some variability in the methodology and confined testing to quasi static conditions.

Conversion to automated programmable motion control creates a number of functions not possible with the previous system. These include:

- Highly repeatable motion profiles independent of the operator
- Determination of the system stiffness under dynamic conditions
- Provide quantitative validation of models of load carriage devices
- Determine the frequency response of LC suspension systems
- Create a automated test cell requiring minimal operator expertise and low cost for possible sale to support other countries modelling efforts

5.2 Purpose

The purpose for this design modification is to support the development of a biomechanical model of human load carriage. The device will initially furnish input values for the dynamic stiffness variables during initial modelling stages. At later stages of the model development, the apparatus can be used to validate the model by comparing the model predicted stiffness responses to a different range of motion profiles.

5.3 Methodology

5.3.1 Hardware Modifications

The test apparatus consists of a human torso shape with independent thorax and pelvic sections. These sections rotate and pivot relative to each other through the required ranges of motion. Previously, this motion was achieved by using a combination of a hinge with an oil lite bearing to allow flexion, and a thrust bearing to allow relative twist. The hinge joint required the operator to loosen a number of locking nuts on two collars and rotate the hinge within the torso and then retighten the locking collars. This hinge had to be aligned parallel to the path of motion of the overhead slider that applies the force to the top of the torso. Even slight misalignments cause increased friction in the joint. This effect had to be compensated for by recording the unloaded force/displacement behaviour of the test apparatus and subtracting this effect from the results of the loaded test. These bearings have been replaced with a custom spherical bearing that allows both twist and flexion and will not require multiple realignments by the operator.

Prior to this upgrade, motion was generated manually using cables and pulleys. Subsequent to this upgrade, the motions of forward and lateral flexion are now fully automated. Linear cyclic motion is generated using a programmable motion control system. This consists of a linear actuator with a 1.25m travel: ERB50-BLTRA20-BSR1250-A, a step and direction servo drive: TQ10SD, a servo motor: SE233BE-KFLG10 and a PC controller card: OEM-AT6400. All components are products of Parker Hannifin Corporation, Automation Division, Cleveland, Ohio. The resistance of a LC system to torsion, forward flexion, and medial/lateral flexion is measured in three separate tests. Originally, moments applied during forward and lateral flexion testing were measured by calculating the difference between the tension in two cables. This required two single axis load cells. This has been replaced with a single bending beam load cell which measures the applied load directly.

Figures 5-1 illustrates the redesigned compliance tester configured for lateral flexion testing. The range of motion required for the lateral flexion test is shown in Figure 5-2.

The long travel of the linear actuator can be used to create a forward flexion of up to 45º. This range is consistent with the forward flexion angle used in previous quasi-static testing. Figure 5-3 shows the configuration and range of displacement of the test apparatus for forward flexion testing. In addition to full range forward flexion testing, it is possible to reproduce the small range forward flexion pattern typical of walking and cycle the test for a fixed duration of time. This gait pattern of dynamic forward flexion could be run multiple cycles and the forward flexion work done by a user could be calculated. Repeating this type of cyclic test for lateral flexion would permit calculation of the lateral flexion work done. If a cyclic torsional test was also performed, the total energy cost of the load carriage system to the user could be estimated. Although originally intended to

test rucksacks, webbing and load carriage vest combinations, the design of the Compliance tester allows many different types of equipment to be tested in this way,

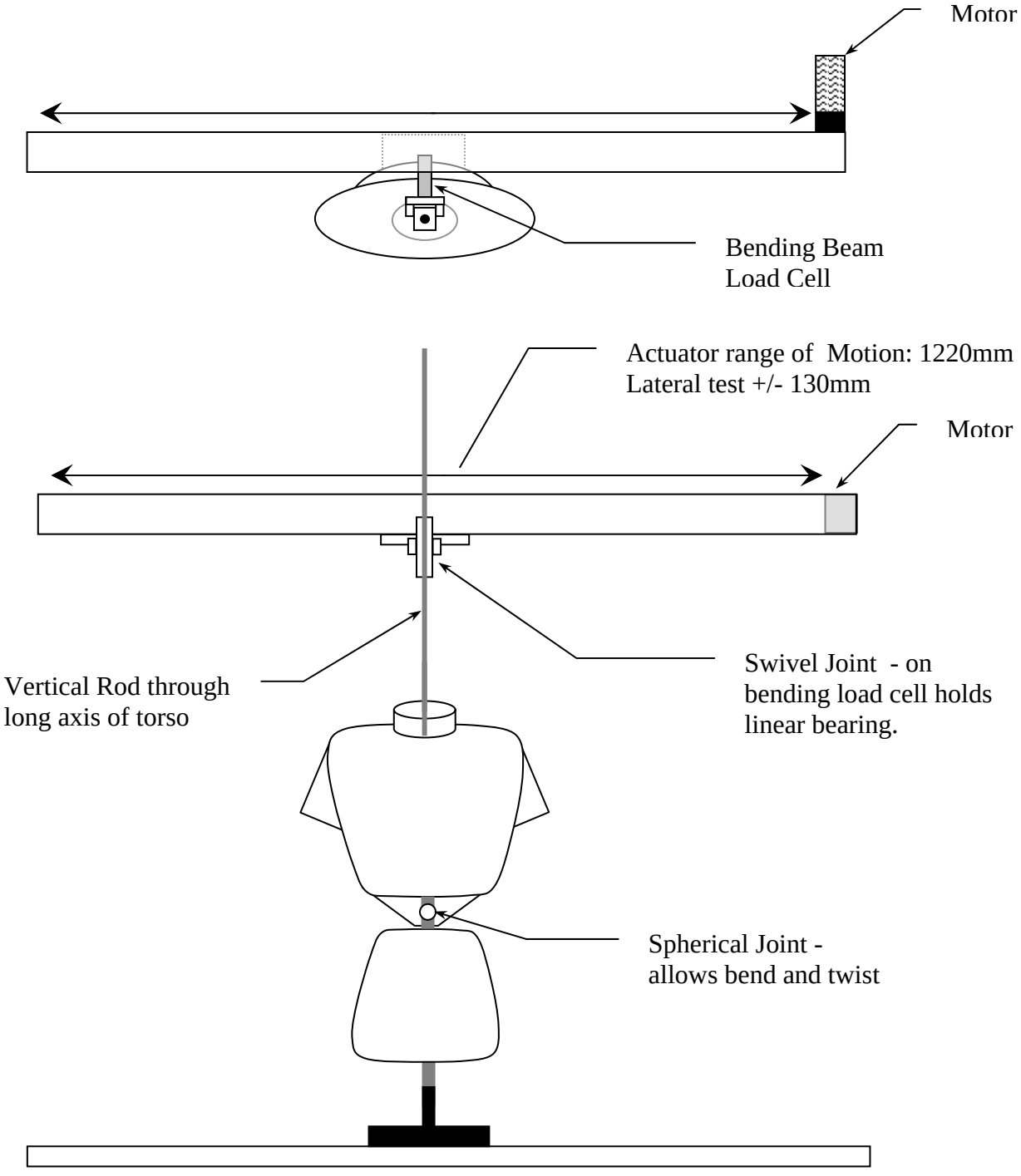

Figure 5-1. Compliance Tester Configured for Dynamic Lateral Flexion Testing: a) Top View and b) Front View.

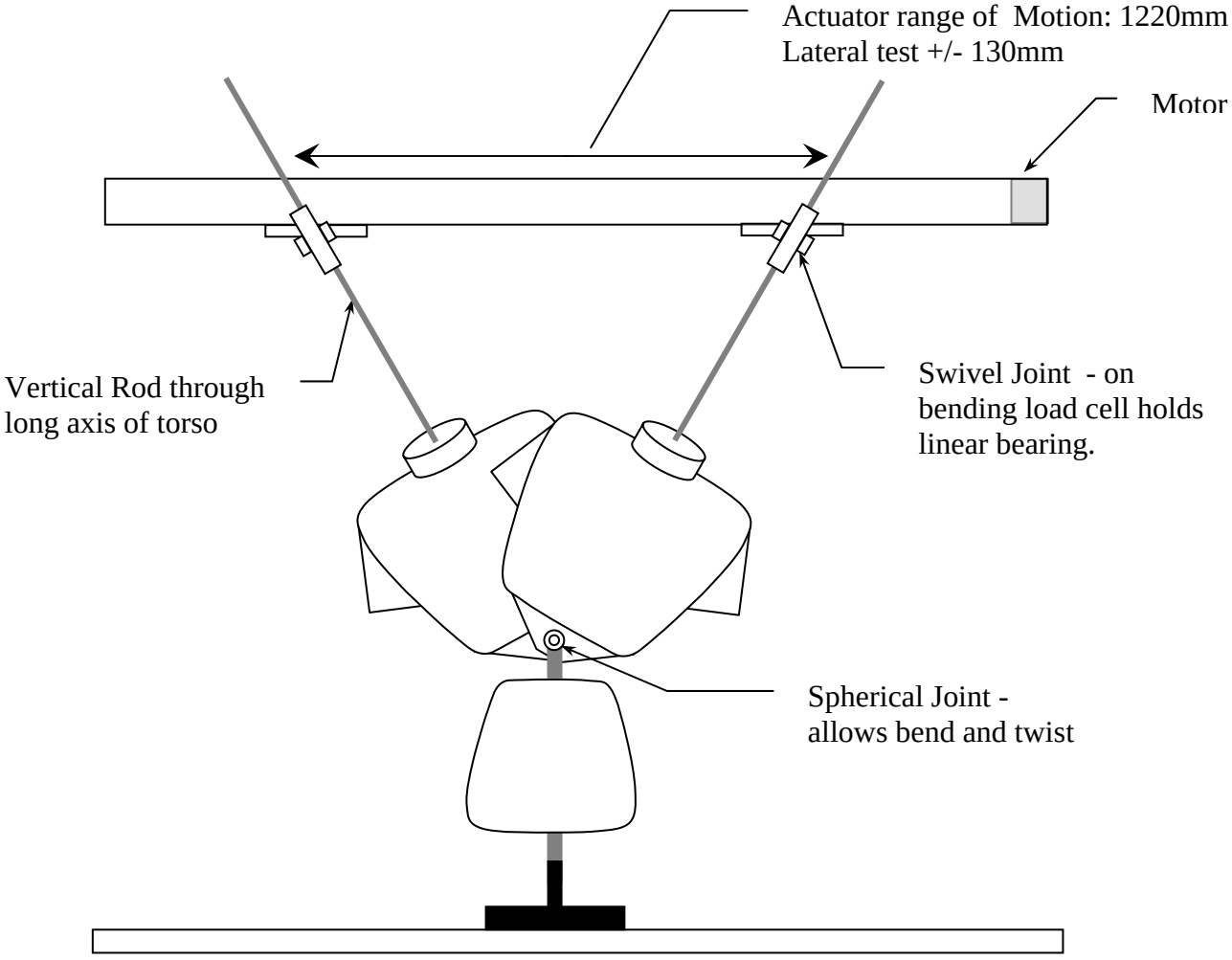

Figure 5-2. Range of Motion during Lateral Flexion Testing
(Default frequency, 1.8 Hz).

including different combinations of clothing layers and or body carried equipment can be assessed. Physiological measures can capture the resultant whole body costs of a "soldier system" while dynamic compliance testing based on human motions can help identify where that work is being done.

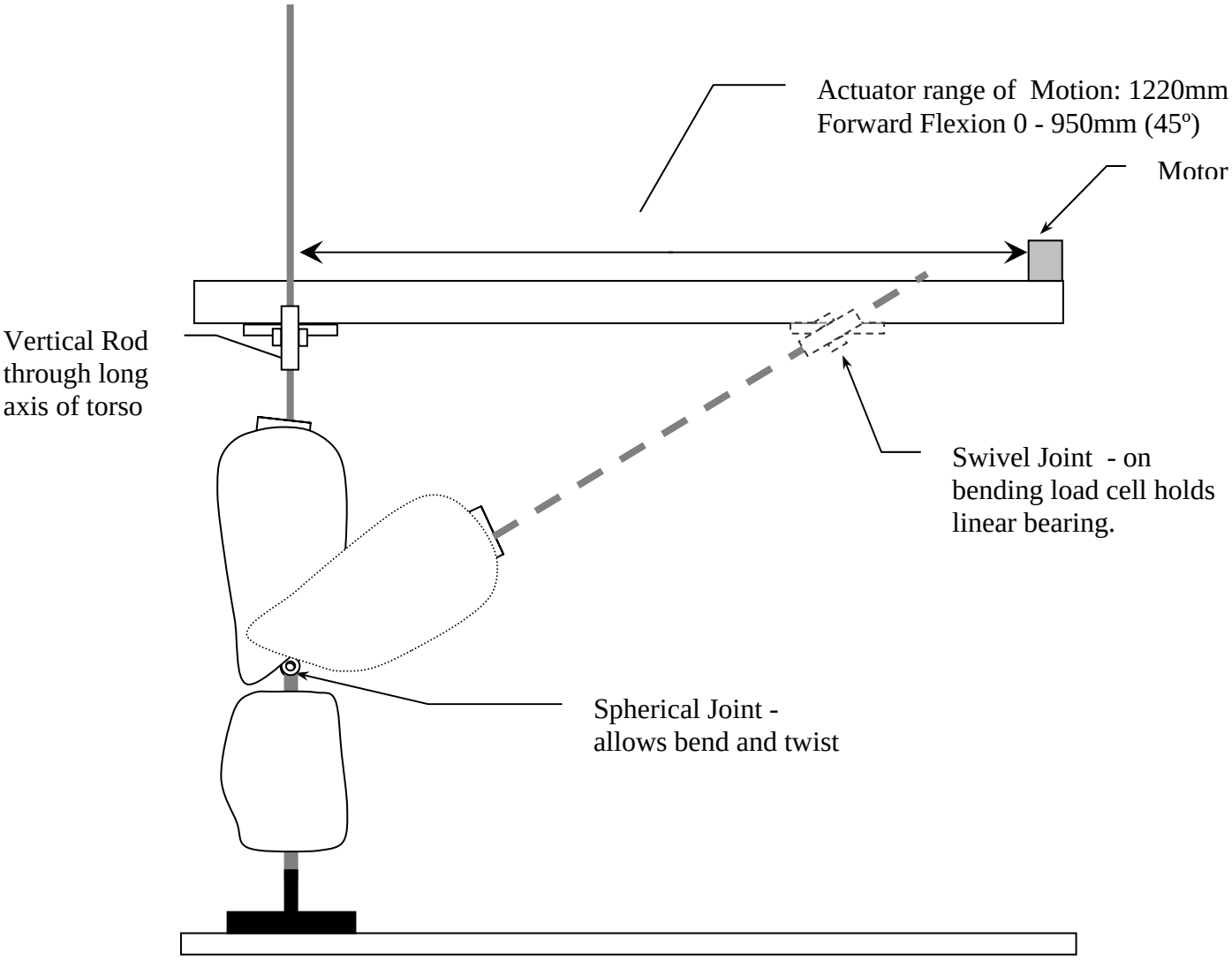

Figure 5-3. Compliance Tester Configuration and Available Range of Motion for forward Flexion Testing

5.2.2 Software Modifications

Data acquisition, motion control and the user interface were realized with LABVIEW V6.1 (National Instruments®) allowing integration of these three functions. This integration greatly reduces the number of operator interventions required during testing. Motions for forward and medial/lateral flexion have been fully automated at this time. An appropriate linkage to automate trunk twist has not been designed as yet, although the data acquisition and user interface for torsional testing have been upgraded. A typical user screen for data acquisition and display during testing appears as Figure 5-4.

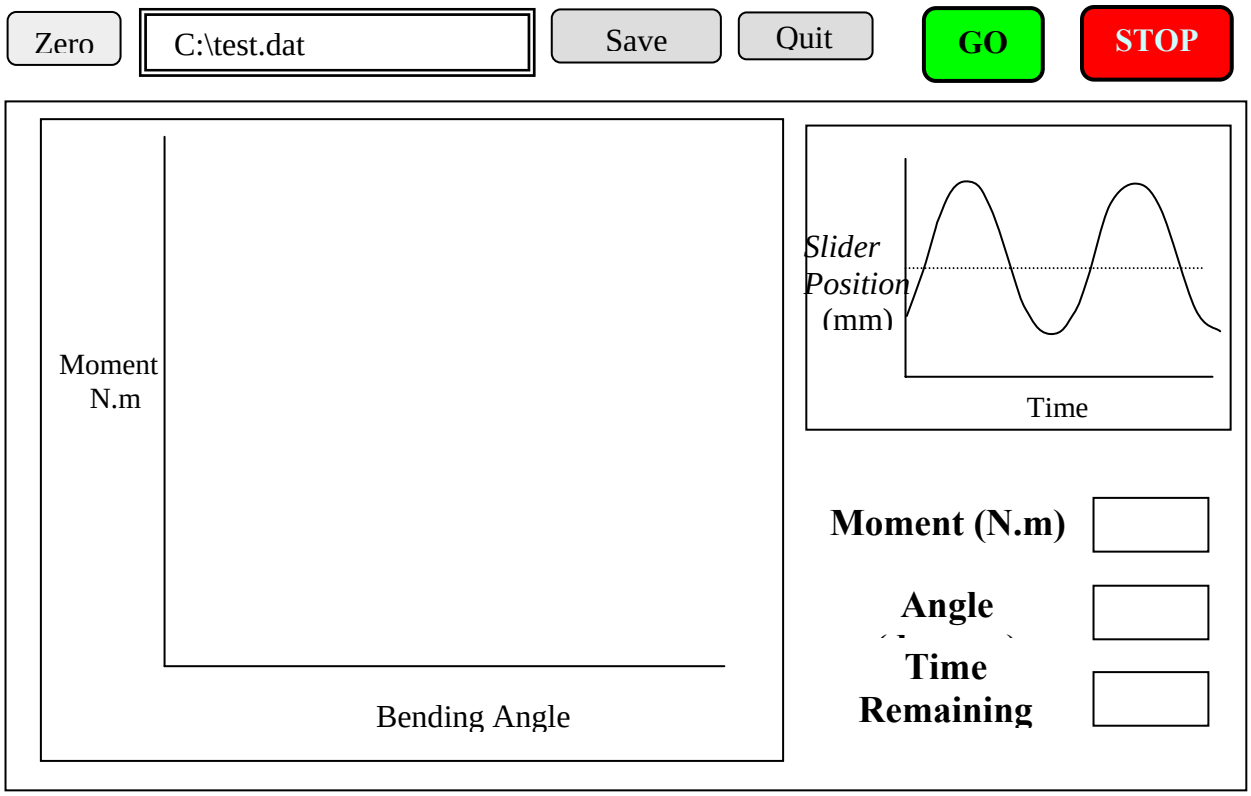

Figure 5-4 Operator Screen (Graphical User Interface)

5.3 Conclusions and Recommendations

The compliance tester has been successfully upgraded to perform programmable dynamic compliance testing in support of ongoing biomechanical modeling of human load carriage. Both the lateral and the forward flexion motions have been successfully automated with a corresponding upgrade to the user interface that permits:

- Highly repeatable motion profiles independent of the operator
- Determination of lateral and forward stiffness under dynamic conditions
- Quantitative validation of analytical models of load carriage devices
- Allow determination of the frequency response of LC suspension systems
- Maintained backwards compatibility, allowing direct comparison to measures taken with the quasi-static design. This maintains the integrity of the existing database.

Additionally, the replacement of the thrust and hinge bearings with a single spherical joint that permits both twist and flexion, reduces the possibility of poor alignment. This change also greatly reduces the level of required operator intervention and expertise. Much of the objective of creating an automated test cell that requires minimal operator expertise has been met.

The final modification required is the design and addition of components that will permit the use of the existing linear actuator to create the rotational motion required for torsional stiffness testing. This will create a complete low cost test apparatus for possible sale to support other countries modelling efforts.

Finally, physiological measures can capture the whole body energy costs of a “soldier system” while the dynamic compliance testing based on human motions can now begin to identify where that work is being done.

6.0 Creation of a Full Body Mapping of the Mannequin

6.1 Introduction

The Phase I static biomechanical model used only pack geometry (the shoulder shape, strap angles, tension and friction ratio of T1/T2 straps) to calculate the shoulder reaction forces (Stevenson et al., 1995). The lumbar reaction force was based on the lean angle and the resultant force needed to maintain static equilibrium. A static model of a waist belt was added in Phase II. This belt was modeled as a partial half cone where the slope of the cone represented the anatomical slope of the hips. The hoop stress equation was used to determine the net compressive force generated by the tension in the waist belt. Net compressive force could then be divided into the lifting and the frictional components. Alan Rigby, in his M.Sc. thesis, attempted to include additional pack elements (i.e. load lifter straps) to improve the model and validate measured waist reaction forces with a load

cell. He found widely ranging frictional forces and variable compliance of the suspension system based on strap tensions. His conclusion was that properly modeling the pack-person interface forces was essential. This thesis served to point the way to a new dynamic modeling approach that deals with the pack-person interface of dynamic suspension systems. It also pointed to the need to find better ways to determine the nature of the pack-person interface.

6.2 Purpose

The purpose of this equipment upgrade was to allow the TekScan™ sensor system to be used as an input to the dynamic biomechanical model. This was accomplished in two ways: 1) to write new software to allow direct access to the raw data from the TeKScan™ thus creating the potential to extract specific contact force histories from Tekscan™ and 2) to develop the ability to determine normal force vectors and locate them in space on the body by conducting a total body mapping of the 50^{th} percentile male mannequin.

6.3 Methodology

In the past we have had concerns with the accuracy of the Tekscan™ pressure measurement system and found errors as high as 15% to 20% in certain conditions, such as bending the Mylar sheet sensors around the shoulder. The system uses electro-conductive ink that carries an electrical current. When a force is applied to the electro-conductive ink, its resistance changes. The Tekscan™ software is designed to record this voltage change, identify the sensor location(s), convert the measured voltage into a force value and, using the known area of the sensel, calculate a corresponding pressure value.

Any variation in the thickness or resistive properties of the ink layer, either because of manufacturing tolerances or due to bending of the sensor will effect the response of the sensel. Tekscan™ software algorithms for calibration and "equilibration" attempt to compensate for the sensel to sensel variation in response. There is also an assumption that the applied force is perpendicular to each sensel which may not be true. Any of these assumptions inherent in the Tekscan™ software calculations can lead to errors. Tekscan pressure outputs continue to be useful to observe 'hot spots', evaluate designs and compare pressure measurements to human tolerance guidelines.

One goal of the new approach in DBM is to use the Tekscan™ pressure measurement system outside the limitations of their commercial clinical software. Tekscan has proven to be very useful in capturing contact pressure distributions and in determining the relative magnitudes of these pressures. The shortcoming of the technology has been its inability to determine the absolute magnitudes of the relative pressures. Tekscan also provides a high spatial resolution at low cost, permitting the user to pinpoint the location of high pressures. If the pressure distribution profiles measured with Tekscan are augmented with the accurate force measurement of the exitsing AMTII load cell in the load distribution mannequin, interface forces can be modeled reliably.

6.3.1 Software

The Tekscan™ software is very sophisticated in handling the massive amounts of data that emerge from sensors which consist of 96 sensels that can be collected at a rate of 200 Hz. One way Tekscan™ manages this process is to provide the user with mainly graphic output (although ASCII output is also available). Our goal was to access the data, including the complete time history, calibrate it and convert it into force values so that the modeling program can use the output from these three dimensional data arrays.

The best method at this time appears to the use a combination of MatLab (a numerical computation and data visualization program) and Microsoft Excel macros. This software-based approach was developed with strong support from research assistants who developed a series of user-friendly data transfer files that began with receiving data from the Tekscan™ system and using Matlab to manipulate the files into the appropriate formats compatible with MSC Visual Nastran™ 4D and 2D Working Model. To allow checking of these data and proper formatting, Excel macros were also used. This software is the pre-modeling engine that will assist us in working outside the Tekscan™ software to create the DBM. The User's Technical Manual, entitled "A User's Guide to LCSim Pressure Data Manipulation" is included as Appendix A.

Excel macros are being used to create a table of force values and the location of the sensel that measured that force. This force array will be needed in two places: first, to map the location of each sensels onto the LC Simulator mannequin and seconding to determine the normal force vector that related to each sensel. Using the location and magnitude of the force vectors, the Tekscan™ system will be used to examine the interaction forces between the pack and the person in dynamic biomechanical modeling. The validation of this approach is the deliverable in Phase II, Part 6b3.

6.3.2 Mapping of the Mannequin

The full body mapping of the 50^{th} percentile mannequin is necessary for several reasons: it will allow us to locate the sensels in 3D space, and it will allow the calculation of the normal reaction force. However, before acquiring the coordinates of the 50^{th} percentile male mannequin, full knowledge of the type of software that would be needed for DBM was required so that the surface model information is stored in an appropriate format. The decision was made to use MSC Software Virtual Nastran 4D modelling and the compatible "Working Model" for rapid 2D analysis (if needed). After that decision, the mannequin was taken to Toronto's Applied Precision Inc. and scanned so that the full body mapping files are now accessible by Visual Nastran 4D for validation of the waist belt model. The resolution of this scan was 2mm and it is shown in the Figure 6-1 below.

Figure 6-1. LC Simulator 50th percentile male mannequin 3D scanned image.

6.4 Anticipated Outcomes

In future stages of the DBM, a standardized lower torso model will be used to validate the approach. As this is a symmetrical form, the results can be derived both mathematically and from a complete Tekscan™ force calculation. The hip belt sensor should capture the resultant force value. For the shoulders, the individual sensing elements can be used to find the normal force vectors and sum them to get the resultant shoulder force vector. This approach can also be used to validate the static biomechanical model's shoulder and waist reaction forces using the normal force from the Tekscan® sensors.

Tekscan™ has a rapid response rate and hence will be very useful for mapping the pack-person interface characteristics. This will be developed as Phase III.

7.0 References

Alexander, R. M. *Elastic Mechanisms in Animal Movement*. Cambridge: Cambridge University Press, 1988.

An, K.N., Jacobsen, M.C., Gerland, L.J., Chao, E.Y.S. Application of a magnetic tracking device to kinesiology studies. *J. Biomech.* 21(7), 613-620, 1988.

Bryant, J.T. Stevenson, J.M., Pelot, R.P., Reid, S.A. and Doan, J.B. (1997) Research and Development of an Advanced Personal Load Carriage System (Phase II and III Section D. PWGSC Contract #W7711-5-7273/001-TOS (27 pages).

Day, J.S., Murdoch, D.J., Dumas, G.A. Calibration of position and angular data from a magnetic tracking device. *J. Biomech.* 33(8):1039-1045, 2000.

DCIEM Contract # W7711-S-7356, Section D – *Development of Acceptance Criteria for Physical Tests of Load Carriage Systems*, 1996.

Ferris, D.P., K. Liang and C.T. Farley. *J. Biomech.* 32:787-794, 1999.

Heglund, N. C., P. A. Willems, M. Penta, and G. A. Cavagna. *Nature* 375: 52-4, 1995.

Inman,V. Ralston, H., Todd, T. *Human Walking*, 1981.

R. Kram and C.R. Taylor. Energetics of running: a new perspective. Nature 346:265-267,1990.

Kram, R. Carrying loads with springy poles. *J. Appl. Physiol.*. 72: 1119-1122, 1991.

Kram, R. Inexpensive load carrying by rhinoceros beetles. J. Experimental Biology 199:609-612,1996.

Kram R., and T.J. Dawson. Energetics and biomechanics of locomotion by red kangaroos (Macropus rufus). Comparative Biochemistry and Physiology, Part B 120:41-49, 1998.

Kram, R. Are efficiency and the cost of generating force both relevant concepts? J. Applied Biomechanics 13:460-463, 1997.

Kram. R. Carrying loads with springy poles. J. Applied Physiology 72:1119-1122, 1991.

Lehman, S.L. R. Kram and C.T. Farley. Locomotion and muscle biomechanics. In: Introduction to Bioengineering (ed. S.A. Berger,W. Goldsmith, E.R. Lewis). U.K.: Oxford University Press, 1996.

Langman, V.A. T.J. Roberts, J. Black, G.M.O. Maloiy, N.C. Heglund, J.-M. Weber,R. Kram and C.R. Taylor. Moving cheaply: energetics of walking in the African elephant. J. Experimental Biology 198:629-632, 1995.

Martin, P.E. and Nelson, R.C. Effects of Gender, Load, and Backpack on the temporal and kinematic Characteristics of Walking Gait. Vol III Natick/TR-82/021, Technical Report, III, 1-78, 1982.

Polhemus Inc. (1995). 3 Space® Users Manual, Colchester, Vermont.

Reid, S.A., Stevenson, J.M., Morin, E.L., Bryant, J.T. (1999) Clothe the Soldier Integrated Load Carriage System: PhaseIIID – Final Design Evaluation using the APLCS Assessment Tools. PWGSC Contract # W7711-8-7461/001/SRV. Report to DCIEM by Queen's University, 46 pages.

Stevenson, J.M. Bryant, J.T. dePencier, R.D., Pelot, R.P., and Reid, J.G. (1995) Research and Development of an Advanced Personal Load Carriage System: Phase I. PWGSC Contract# W7711-4-7225/01-XSE. Report to DCIEM by Queen's University, 250 pages.

Stevenson, J.M., Bryant, J.T., Reid, S.A., Doan, J.E.B. (1996). Validation of the Load Carriage Simulator: Phase D. within Research and development of an Advanced Personal Load Carriage System. PWGSC Contract# W7711-4-7225/01-XSE. Report to DCIEM by Queen's University, 49 pages.

Appendices

Appendix A – Moment of Inertia Governing Equations

The following equation is used to solve the moment of inertia:

$$I = \frac{0.2485 r^2}{l}\left(mT^2 - m_p T_p^2\right)$$

Where :

$I = \text{mass moment of inertia } (kg \cdot m^2)$

$m = \text{mass of plate/object combination } (kg)$

$T = \text{period of plate/object combination } (s)$

$m_p = \text{mass of plate } (kg)$

$T_p = \text{period of plate } (s)$

$r = \text{effective radius of plate } (m)$

$l = \text{length of filaments } (m)$

Appendix B – Centre of Gravity Location of a Measured Object

Figure 4-3. The top-view photos are manipulated with drawing software, such as CorelDraw. The intersection of the red lines indicates the centre of gravity of the object in that view.

If the proposed laser light assembly is used, these steps are not required. The object can be physically marked at the point where the centered laser light shines.

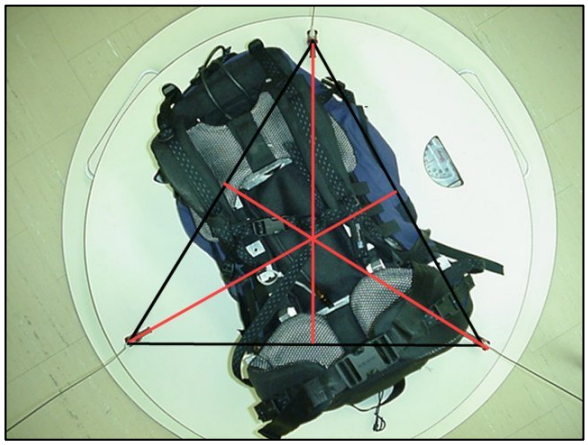

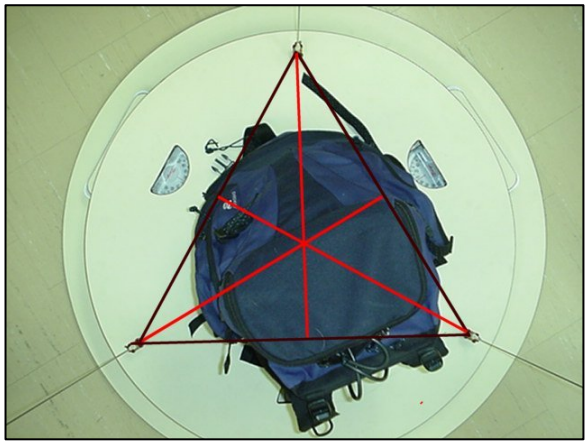

Appendix C – Design Calculations

Radius of Plate

The radius dimension was chosen after measuring various backpacks and surveying the current researchers of the Queen's Ergonomic Research Group backpack project.

The widest object the plate can take is equal to 2/3 of the height of the triangle formed by the cable attachment points.

The effective diameter of the plate was chosen to be 88.9cm.
Therefore, the effective radius is 44.5cm.

Calculation of Ideal Cable Length

r/L = constant

Where r is the effective radius of the plate, and L is the length of the wire.

For the current (proven) pendulum in Jackson Hall r/L=(24.9cm)/(192.4cm) = 0.13

New pendulum: L=r/0.13 = (44.5cm)/0.13 = 342.9cm

Appendix D – Calibration

Calibration of Weigh Scales

The calibration concurred with the manufacturer's error factor of +/-1lb.

Weight (lb)	Scale A	Scale B	Scale C
5	5.5	5	5
	6	5	5
	5.5	5	5
10	11	10	10
	10	10	9.5
	10	10.5	10
20	20	20	19.5
	20	20	20
	20	20	20
40	41	40	40
tared	40	40	39.5
	40.5	40	40
5	5	5.5	5
	5	5	5
	5	5	5
10	10.5	10	9.5
	10.5	10	10
	10.5	10	9.5
20	20	20	19
	20	19.5	19
	20	20	19.5
40	40	39	39
	40	40	40
	40	40	39.5
120	121	121	120
tared	120.5	120	119
	120	120	119
10	10	9.5	10
	9.5	9.5	10
	10	10	9.5

Calibration of Pendulum

The inertia of the empty pendulum was measured and compared with a mathematically calculated value. The pendulum was then calibrated with a solid object, 31.4cm high, 38.1cm wide, 19cm long. The mass was 17.1kg.

Constants				
	Imperial		Metric	
mass p=	22.5	lb	10.2	kg
total mass=	60	lb	27.3	kg
T (plate)=	2.99	s	2.99	s
l (filaments)=	135	inches	3.43	m
r (plate)=	17.5	inches	0.445	m
g=			9.81	m/s2

Empty Plate				With Object				
Time for 10 rotations					Time (s) for 10 rotations			
1	29.97				Trial 1	Trial 2	Trial 3	
2	29.78			1	19.92	19.78	19.73	
3	29.79			2	19.95	19.75	20.19	
4	29.91			3	19.81	19.96	19.81	
5	29.81			4	19.93	19.88	19.76	
6	30.03			5	19.79	19.99	19.73	
7	29.84			6	19.81	19.73	19.83	
8	30.01			7	20.03	20.09	19.92	
9	30			8	19.92	19.77	19.86	
10	29.98			9	19.86	19.75	19.79	
11	29.96			10	19.76	19.93	19.85	
12	29.91							
				Total	198.78	198.63	198.47	
	358.99			Avg Period (s)	1.9878	1.9863	1.9847	
	29.9158							
Period	2.99158			Mom of Inertia	0.239333892	0.236999	0.234511	kgm^2
I of plate alone (measured)				Calculated I	0.257	kgm^2		
I=	1.30821	kgm^2						
Calculated I	1.01	kgm^2						

Statistical Analysis of Measured Periods During Calibration

Anova: Two-Factor Without Replication

SUMMARY	*Count*	*Sum*	*Average*	*Variance*
Row 1	3	59.43	19.81	0.0097
Row 2	3	59.89	19.96333	0.048533
Row 3	3	59.58	19.86	0.0075
Row 4	3	59.57	19.85667	0.007633
Row 5	3	59.51	19.83667	0.018533
Row 6	3	59.37	19.79	0.0028
Row 7	3	60.04	20.01333	0.007433
Row 8	3	59.55	19.85	0.0057
Row 9	3	59.4	19.8	0.0031
Row 10	3	59.54	19.84667	0.007233
Column 1	10	198.78	19.878	0.007307
Column 2	10	198.63	19.863	0.015623
Column 3	10	198.47	19.847	0.018112

ANOVA

Source of Variation	*SS*	*df*	*MS*	*F*	*P-value*	*F crit*
Rows	0.137853	9	0.015317	1.19082	0.357854	2.456282
Columns	0.004807	2	0.002403	0.186847	0.831159	3.554561
Error	0.231527	18	0.012863			
Total	0.374187	29				

	Column1
Mean	19.86266667
Standard Error	0.020738843
Median	19.84
Mode	19.92
Standard Deviation	0.113591322
Sample Variance	0.012902989
Kurtosis	1.01809769
Skewness	1.051352803
Range	0.46
Minimum	19.73

Maximum	20.19
Sum	595.88
Count	30
Confidence Level(95.0%)	0.04241572

Appendix D, Annex #1: Calibration Graphs of Miniature Sensors

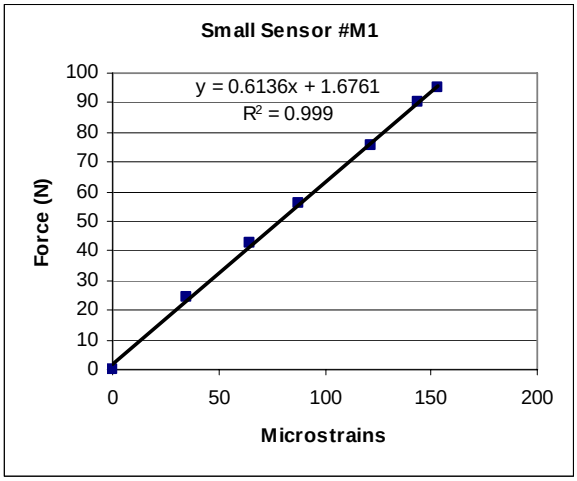

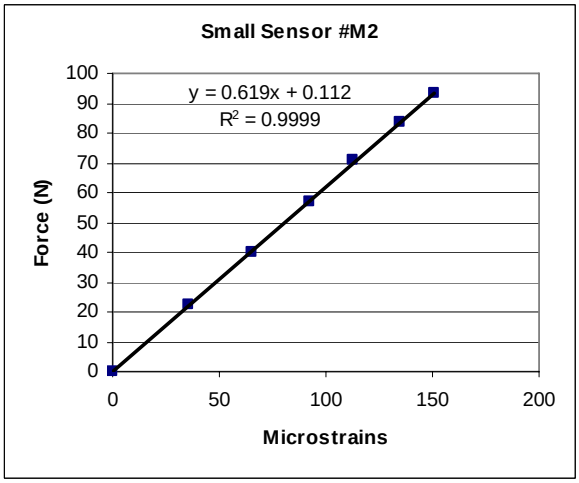

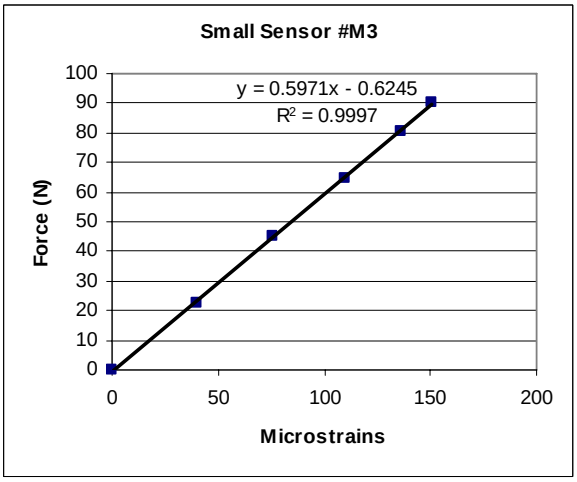

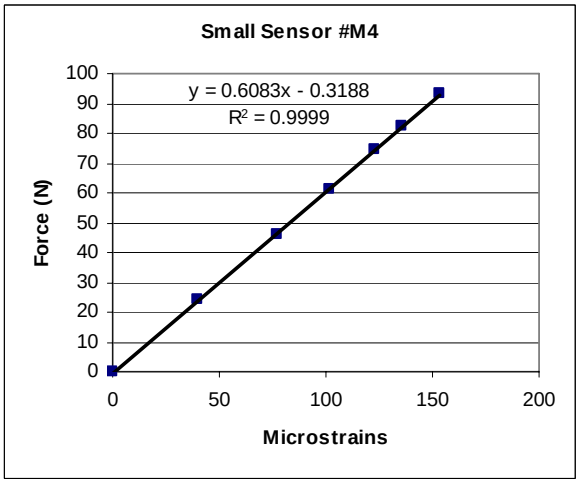

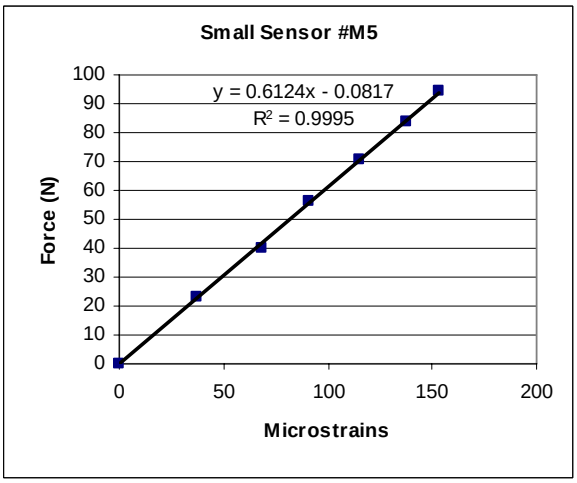

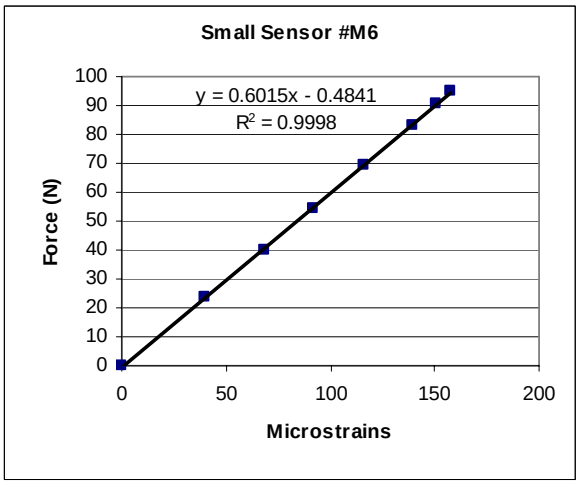

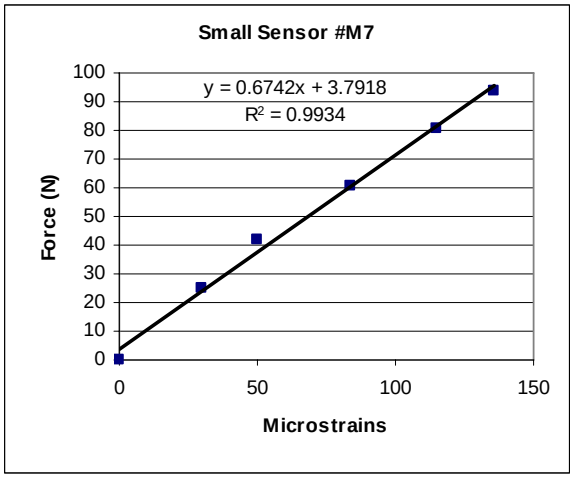
Small Sensor #M7
y = 0.6742x + 3.7918
R² = 0.9934
Force (N)
Microstrains
0
10
20
30
40
50
60
70
80
90
100
0
50
100
150

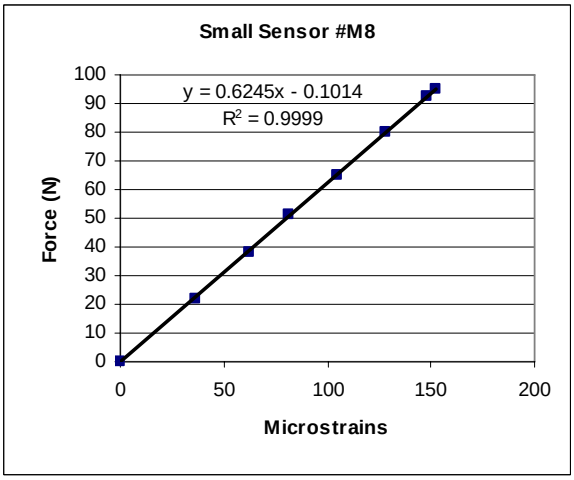
Small Sensor #M8
y = 0.6245x - 0.1014
R² = 0.9999
Force (N)
Microstrains
0
10
20
30
40
50
60
70
80
90
100
0
50
100
150
200

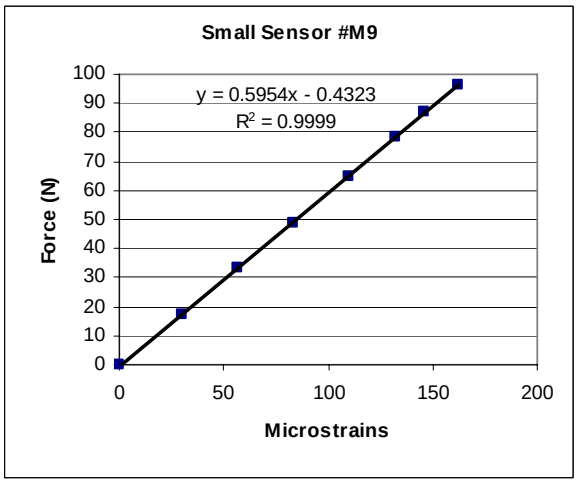
Small Sensor #M9
y = 0.5954x - 0.4323
R² = 0.9999
Force (N)
Microstrains
0
10
20
30
40
50
60
70
80
90
100
0
50
100
150
200

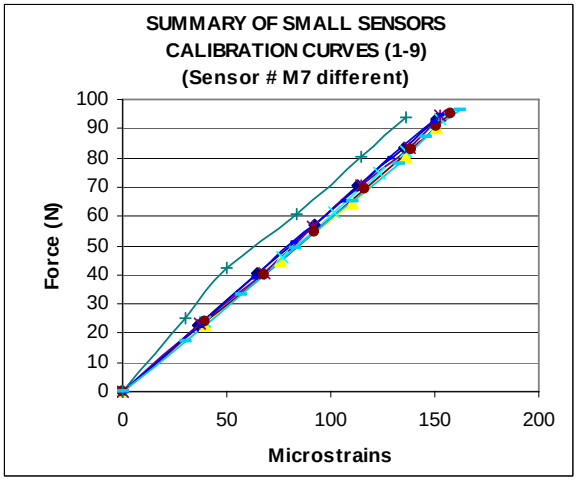
SUMMARY OF SMALL SENSORS
CALIBRATION CURVES (1-9)
(Sensor # M7 different)
Force (N)
Microstrains
0
10
20
30
40
50
60
70
80
90
100
0
50
100
150
200

Appendix E – Centre of Gravity Finder Calculations

Trial	1											
x	y	x calc	y calc	Diff x	Diff y	off by	A	B	C	Sum		
15	0	14.4	-0.3	-0.6	-0.3	0.7	26	2	1.5	29.5		
10	0	8.8	0	-1.2	0	1.3	20	5	5	30		
5	-5	4.2	-5.2	-0.8	-0.2	0.9	15	13	2.5	30.5		
5	0	4.4	-0.5	-0.6	-0.5	0.8	15	8	7	30		
5	5	4.4	4.5	-0.6	-0.5	0.8	15	3	12	30		
0	-10	0	-10.1	0	-0.1	0.1	10	20	0	30		
0	-5	0	-6.1	0	-1.1	1.1	10	16	4	30		
0	0	-0.1	-0.2	-0.1	-0.2	0.3	10	11	10	30.5		
0	5	-0.3	4.6	-0.3	-0.4	0.5	10	5.5	15	29.5		
0	10	-0.7	10	-0.7	0	0.7	9	0.5	20	29.5		
-5	-10	-5.3	-10.7	-0.3	-0.7	0.7	4	24	2.5	30.5		
-5	-5	-4.5	-4.6	0.5	0.4	0.6	5	16	7.5	28		
-5	0	-5	0	0	0	0	4	12	12	28		
-5	5	-4.5	5.5	0.5	0.5	0.7	5	6.5	17	27.5		
-5	10	-5.1	8.9	-0.1	-1.1	1.1	4	4	21	29		
					Avg off by=	0.68						
Trial	2											
x	y	x calc	y calc	Diff x	Diff y	off by	A	B	C	Sum		
15	0	14.9	-0.5	-0.1	-0.5	0.5	27	2	1	30		
10	0	8.9	-0.5	-1.1	-0.5	1.2	21	5.5	4.5	30.5		
5	-5	4.8	-5.2	-0.2	-0.2	0.3	15	12	2	29		
5	0	4.8	0	-0.2	0	0.2	15	7	7	29		
5	5	4.8	5.2	-0.2	0.2	0.3	15	2	12	29		
0	-10	0.3	-9.9	0.3	0.1	0.3	11	20	0	30.5		
0	-5	0	-5.1	0	-0.1	0.1	10	15	5	30		
0	0	0	0	0	0	0	10	10	10	30		
0	5	0	4.8	0	-0.2	0.2	10	5	14	28.5		
0	10	0.1	9.5	0.1	-0.5	0.5	10	0.5	19	29.5		
-5	-10	-5	-11.9	0	-1.9	1.9	4	23	1	28		
-5	-5	-5.1	-5.7	-0.1	-0.7	0.8	4	18	7	29		
-5	0	-4.2	1	0.8	1	1.3	5	11	13	29		
-5	5	-4.6	4.6	0.4	-0.4	0.6	5	8.5	18	31.5		
-5	10	-5.2	10	-0.2	0	0.2	4	3	23	29.5		
					Avg off by=	0.55						

Trial	3											
x	y	x calc	y calc	Diff x	Diff y	off by	A	B	C	Sum		
15	0	15.6	0	0.6	0	0.6	26	1	1	28		
10	0	10.7	0	0.7	0	0.7	20	3.5	3.5	27		
5	-5	5.6	-4.9	0.6	0.1	0.7	17	12	2	31		
5	0	5.9	-0.2	0.9	-0.2	0.9	17	7	6.5	30.5		
5	5	5.3	5.1	0.3	0.1	0.3	16	2	12	30		
0	-10	0.6	-9.8	0.6	0.2	0.6	11	20	0	31		
0	-5	0	-6.1	0	-1.1	1.1	10	16	4	30		
0	0	0.3	-0.5	0.3	-0.5	0.6	10	10	9	29		
0	5	0.3	4.7	0.3	-0.3	0.4	10	5	14	29		
0	10	0.1	10	0.1	0	0.1	10	0	20	29.5		
-5	-10	-5.4	-9.3	-0.4	0.7	0.8	4	23	4	31		
-5	-5	-5.1	-4.7	-0.1	0.3	0.4	5	19	9	32.5		
-5	0	-5.5	0	-0.5	0	0.5	4	14	14	32		
-5	5	-4.5	4.9	0.5	-0.1	0.5	5	8	18	31		
-5	10	-4.4	9.6	0.6	-0.4	0.7	5	3	22	30		
					Avg off by=	0.59						
Averages												
x	y	X1	X2	X3	Mean	off x	Y1	Y2	Y3	Mean	off y	Total off
15	0	14.4	14.9	15.6	15	-0.03	-0	-1	0	-0.27	-0.3	0.26
10	0	8.8	8.9	10.7	9.47	-0.53	0	-1	0	-0.17	-0.2	0.58
5	-5	4.2	4.8	5.6	4.87	-0.13	-5	-5	-5	-5.1	-0.1	0.17
5	0	4.4	4.8	5.9	5.03	0.03	-1	0	-0	-0.23	-0.2	0.25
5	5	4.4	4.8	5.3	4.83	-0.17	5	5.2	5.1	4.933	-0.1	0.19
0	-10	0	0.3	0.6	0.3	0.3	-10	-10	-10	-9.93	0.07	0.29
0	-5	0	0	0	0	0	-6	-5	-6	-5.77	-0.8	0.73
0	0	-0.1	0	0.3	0.07	0.07	-0	0	-1	-0.23	-0.2	0.26
0	5	-0.3	0	0.3	0	0	5	4.8	4.7	4.7	-0.3	0.3
0	10	-0.7	0.1	0.1	-0.17	-0.17	10	9.5	10	9.833	-0.2	0.21
-5	-10	-5.3	-5	-5.4	-5.23	-0.23	-11	-12	-9	-10.6	-0.6	0.67
-5	-5	-4.5	-5.1	-5.1	-4.9	0.1	-5	-6	-5	-5	0	0.07
-5	0	-5	-4.2	-5.5	-4.9	0.1	0	1	0	0.333	0.33	0.36
-5	5	-4.5	-4.6	-4.5	-4.53	0.47	6	4.6	4.9	5	0	0.48
-5	10	-5.1	-5.2	-4.4	-4.9	0.1	9	10	9.6	9.5	-0.5	0.51
											Avg off=	0.36

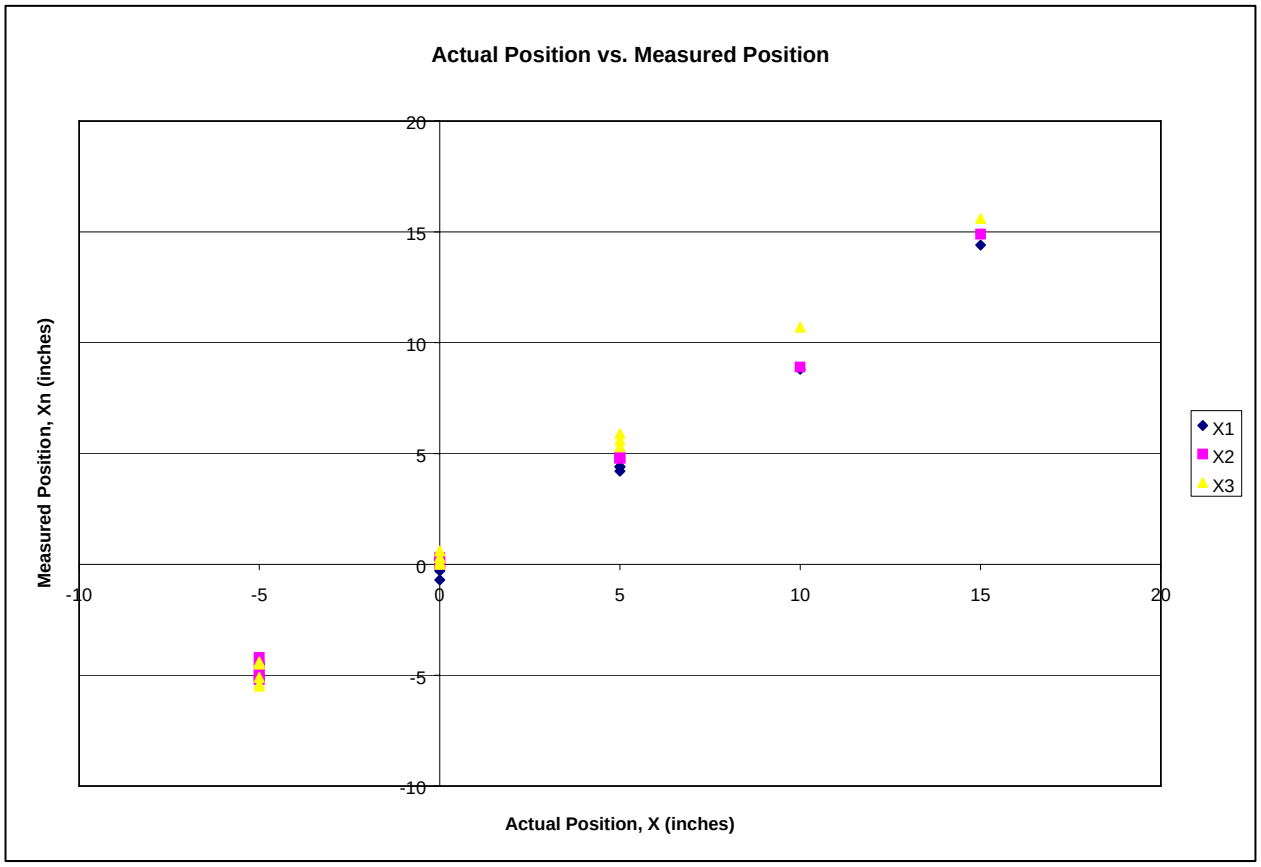
Actual Position vs. Measured Position
Measured Position, Xn (inches)
20
15
10
5
0
-5
-10
-10
-5
0
5
10
15
20
Actual Position, X (inches)
X1
X2
X3

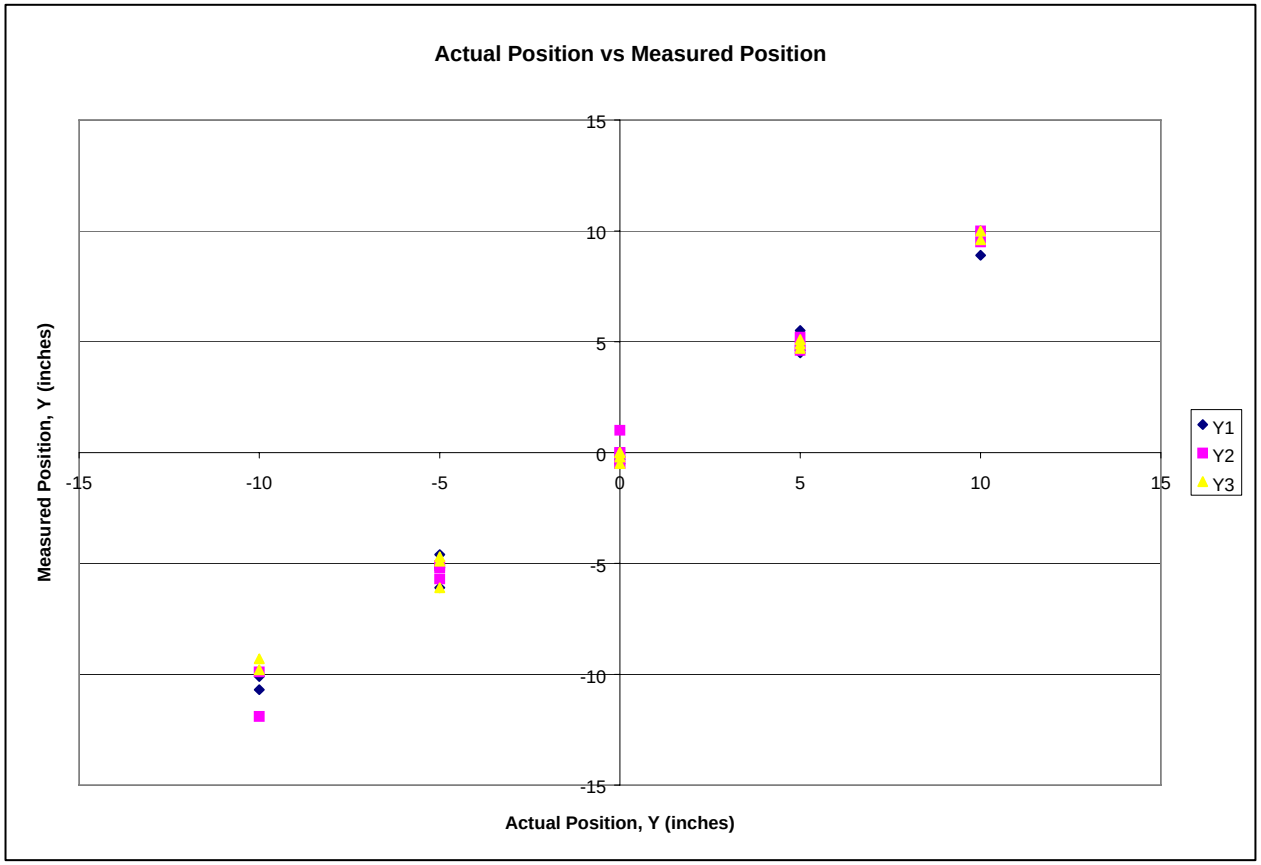
Actual Position vs Measured Position
Measured Position, Y (inches)
15
10
5
0
-5
-10
-15
-15
-10
-5
0
5
10
15
Actual Position, Y (inches)
Y1
Y2
Y3

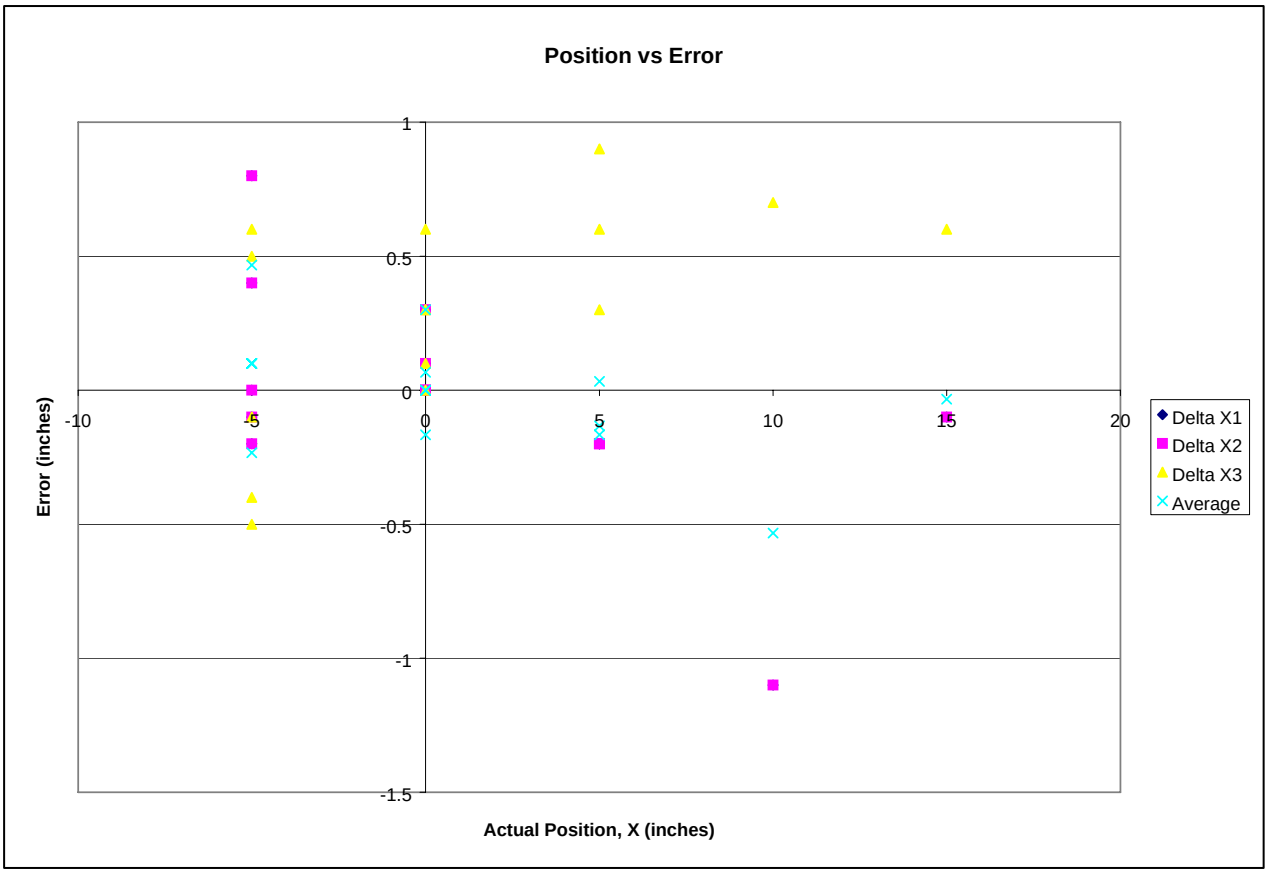
Position vs Error
Error (inches)
1
0.5
0
-0.5
-1
-1.5
-10
-5
0
5
10
15
20
Actual Position, X (inches)
Delta X1
Delta X2
Delta X3
Average

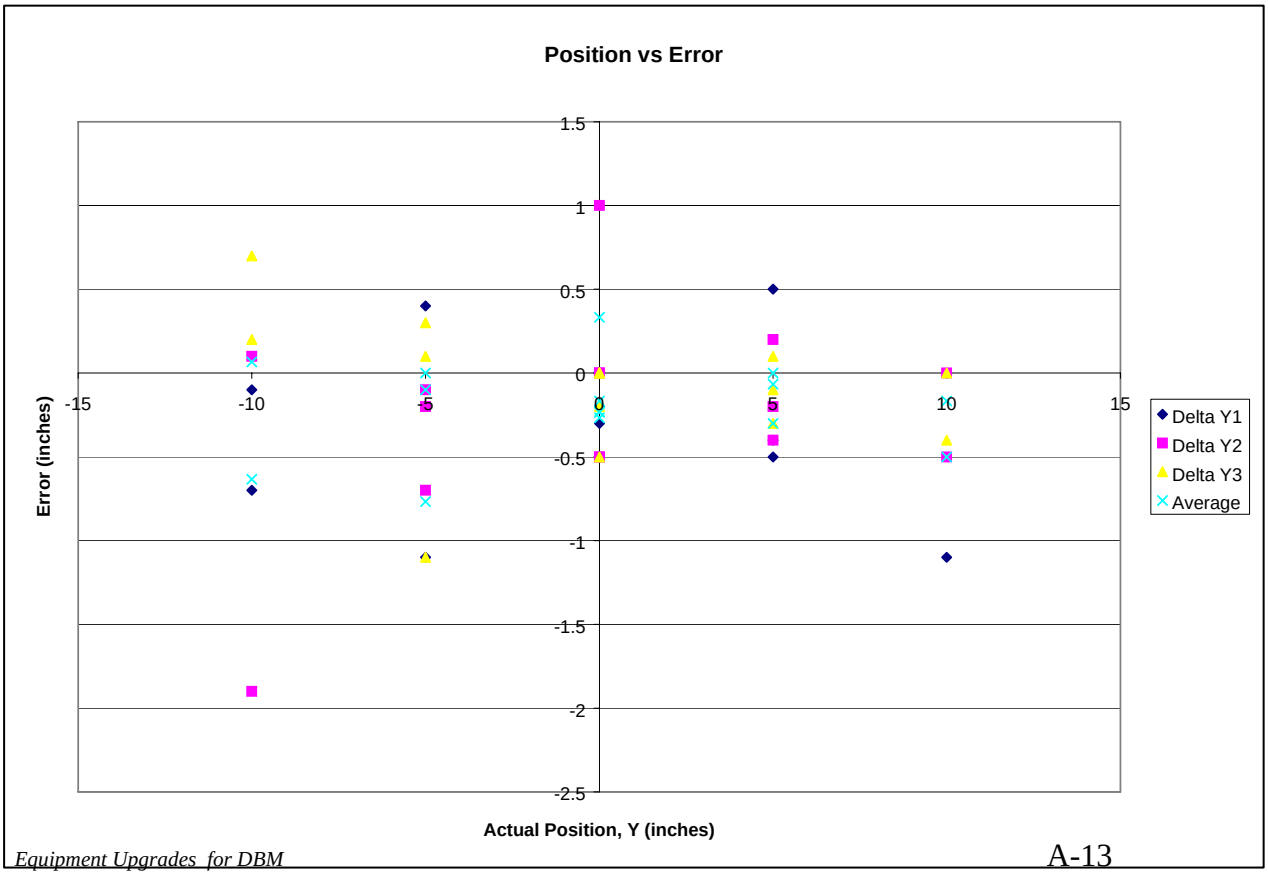
Position vs Error
Error (inches)
1.5
1
0.5
0
-0.5
-1
-1.5
-2
-2.5
-15
-10
-5
0
5
10
15
Actual Position, Y (inches)
Delta Y1
Delta Y2
Delta Y3
Average

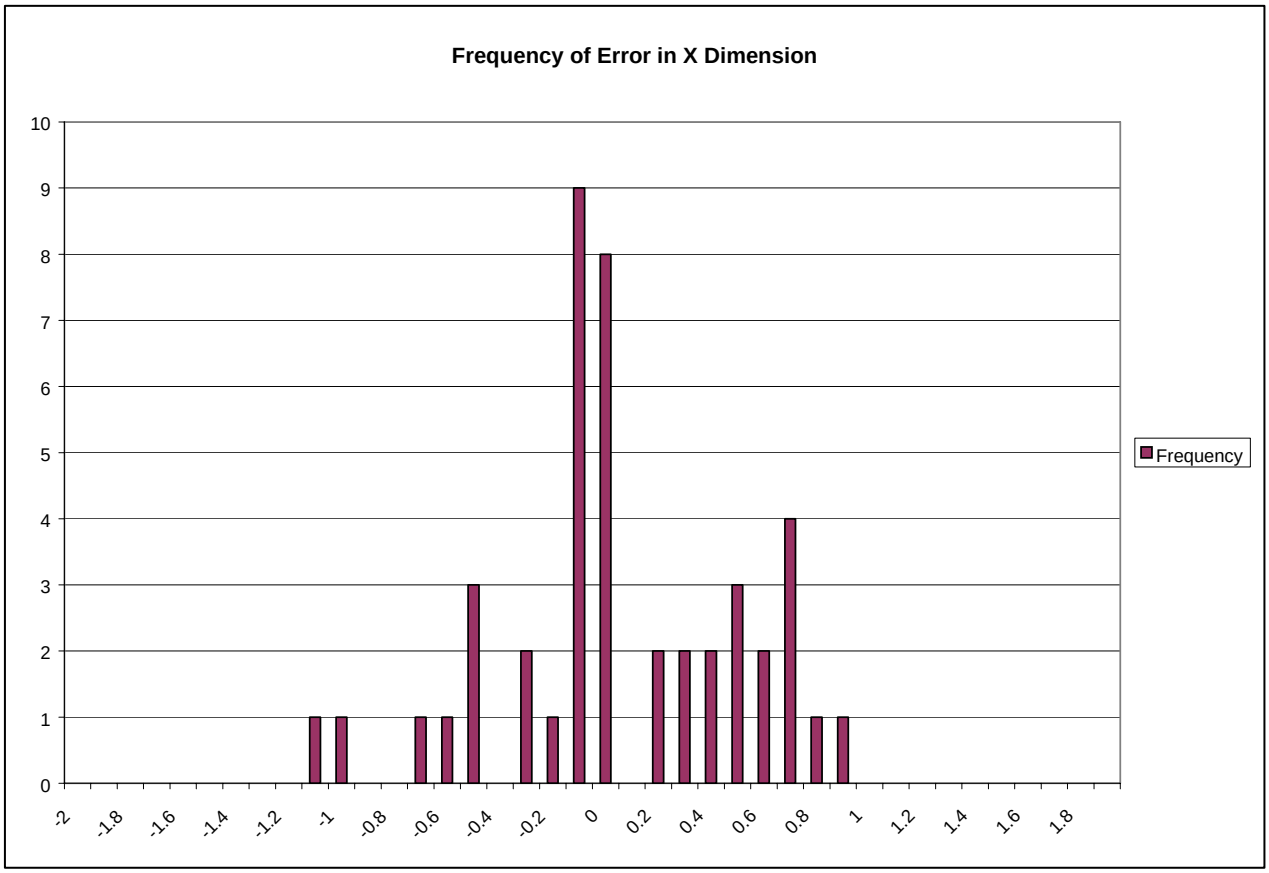
Frequency of Error in X Dimension
10
9
8
7
6
5
4
3
2
1
0
-2
-1.8
-1.6
-1.4
-1.2
-1
-0.8
-0.6
-0.4
-0.2
0
0.2
0.4
0.6
0.8
1
1.2
1.4
1.6
1.8
Frequency

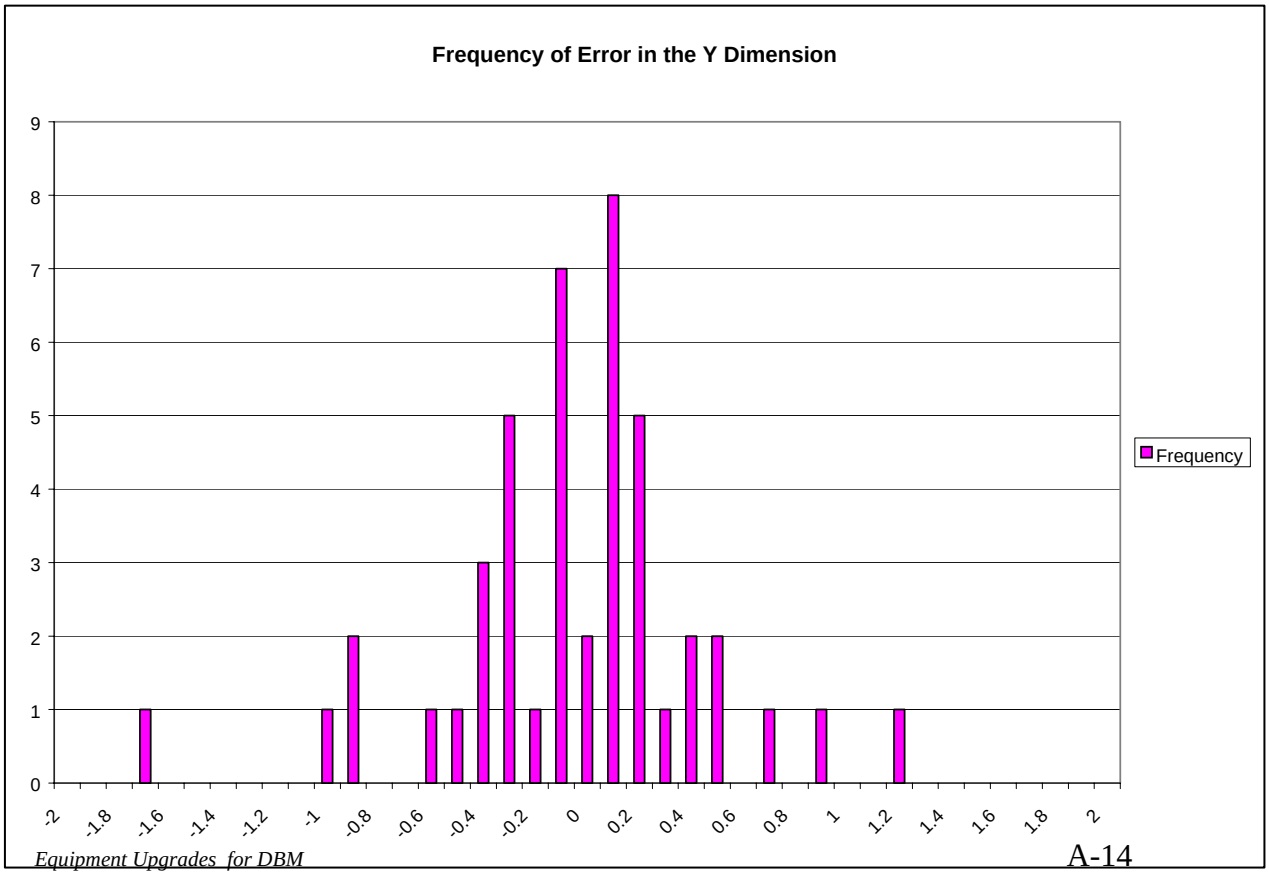
Frequency of Error in the Y Dimension
9
8
7
6
5
4
3
2
1
0
-2
-1.8
-1.6
-1.4
-1.2
-1
-0.8
-0.6
-0.4
-0.2
0
0.2
0.4
0.6
0.8
1
1.2
1.4
1.6
1.8
2
Frequency

Appendix F - User's Guide for the LCSim Pressure Data Manipulator

Developed by Sabrina DiVinceza and Michael Hadrovic
Department of Mathematics and Statistics
2001

WHAT IS THE FUNCTION?

The LCSim Pressure Data Manipulator is a MATLAB Graphical User Interface, which is designed to aid in the analysis of Tekscan Data, collected from the Load Carriage Simulator. The GUI calls upon a toolbox of MATLAB .m-files to accomplish this.

WHERE IS ALL THIS STUFF?

There are several MATLAB functions that the LCSim Pressure Data Manipulator uses to accomplish the analysis of the fscan pressure data. They are located on APLCS#5 in the following directory, 'c:\sab&mike\sab_mike\'.

Their filenames are:

averagemax.m
averagemin.m
cofmass.m
dudes_wk1write.m
peaklocation.m
plotpeak.m
senselaverage.m
senselmax.m
setfile.m
thesis_menu.m

Also used are the two .m-files that were provided by Tekscan to load the data into MATLAB. Loadfsx.m (edited slightly) and exstr.m are located in the directory 'c:\sab&mike\Matlabfsx\'.

The Macros which format the spreadsheets created by the manipulator are located in the excel file 'thesis_VBmacros.xls', which is in the directory 'c:\sab&mike\'.

'Installing' the Data Manipulator

APLCS#5 has MATLAB on it, and the path settings have been changed so that MATLAB knows where all the necessary .m-files are. The Data Manipulator can be used on any computer with MATLAB installed (it was created initially for MATLAB version 5.2), as long as the .m-files listed above are on that computer and you tell MATLAB where they are.

To do this, open MATLAB, choose the 'File' menu, and choose 'Set Path...' to open the Path Browser. In the Path Browser, click on the 'Path' menu button, choose 'Add to Path…' and enter the directory where the .m-files are stored. Once you've done this for all the directories, MATLAB will be ready to go.

Starting the Manipulator

To begin using the Data Manipulator, just type 'thesis_menu' in the MATLAB command window. This brings up the GUI from which you perform all the operations available in the suite.

Features of the GUI

Please refer to "Graphical Users Interface" shown in Figure 6–2
The column of buttons on the left side of the GUI window is used to execute the different functions.

- There is a grey box in the middle of the window. This is the description box. After clicking on one of the buttons, this box will display an explanation of the function you just used.
- Below that grey box, there is another. This is the system message box. This box will display messages regarding what the manipulator is doing. It will let you know about things that are happening, but aren't popping up in front of your face.
- The button in the bottom right corner is the mystery button. See if you can figure out what it does.
- Above this, there are a bunch of yellow boxes. These display information about the data file you currently have loaded.
- Above these yellow boxes are two input boxes where the user can define the threshold pressure and the mannequin frequency. These values are used in various functions.
- To the right of the 'Plot Peak' button, there is a drop list. This list contains plotting options only used with the 'Plot Peak' function.
- Finally, the input box at the top, to the right of the Load .fsx Data button, is the file box. This is where the user enters the path of the data file they want to work with.

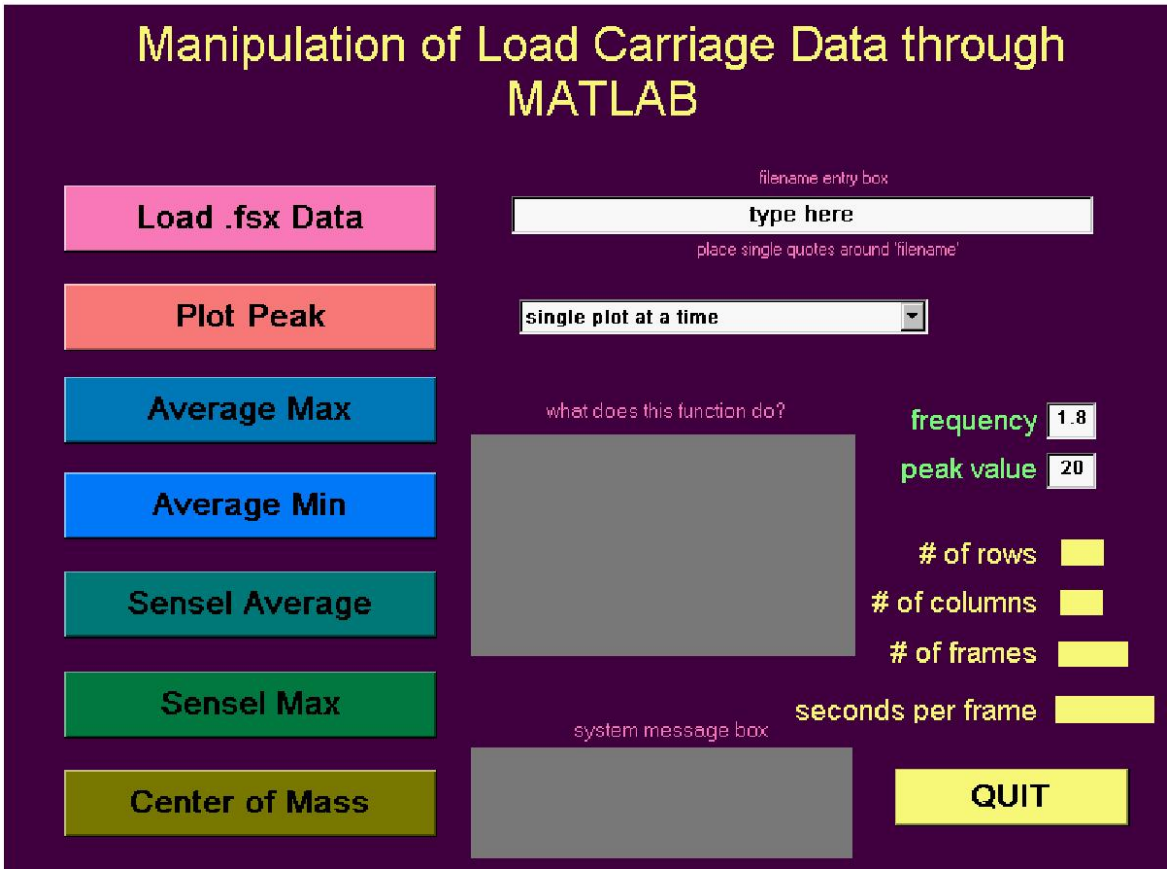

Figure 6-2 Graphical Users Interface (GUI) for LCSim Pressure Data Manipulator

CHOOSING A FILE TO WORK WITH

To begin using the functions, you must first choose a data file to work with. Enter the filename in the filename box located in the upper right of the GUI. Be sure to include the entire path, the file extension, and to place single quotes around the whole thing.

Example: in the input box, type 'c:\sab&mike\data.fsx' to use a data file in that location.

Once the name is entered, click on the 'Load .fsx Data' button. This will import the data file into MATLAB and make it the active file. The results of the load, including whether it was a success or failure, will appear in the MATLAB command window. Now you're ready to poke at the data with other functions. If you want to work with a different file, just repeat these steps with the new filename.

WHAT ABOUT USING THE DIFFERENT FUNCTIONS?

Assuming you were successful in loading a data file, before you actually start analyzing the data you must enter the mannequin frequency. This is done using the frequency input box, which is located just above the yellow info boxes on the right. It requires manual entry of the frequency at which the mannequin was cycled up and down during the trial from which the data was gathered. The default value in the box is 1.8. The value entered will be understood to be in Hz.

Also, be sure to pay attention to the description box and the system message box when running any of the functions. They will indicate when there is important information in the MATLAB command window, as well as the names of spreadsheet files that have been created by the functions.

Plot Peak

Activated with the button of the same name, the Plot Peak function plots a graph of pressure vs. time for sensels that attained the threshold pressure at some point during the trial.

To use this function you must first set the threshold pressure. This is done in the input box marked 'peak value' on the right side of the GUI window. The default value in the field is 20.

Next, using the drop-menu of plotting options, choose the type of plot you'd like to see. Once you've done this, you can run 'Plot Peak' by clicking the button. While the function is displaying the data it may also need you to tell it what to do by pressing certain keys. It will request this in the MATLAB command window.

If the function is run with the 'multi-view single plots' option chosen, it will create a figure full of little graphs, each one corresponding to a different sensel. Choosing 'single plot at a time' will place the data for each sensel in its own figure. The function will pause after it creates each one and to get the next, you must press <enter> (notice you were directed by the system message box to check the command window). If you choose 'multiple plots per graph', you will get figures with one graph on them, but there will be as many as three lines on the graph, each representing a different sensel. Remember to check the command window to see if there are more figures to display.

Average Max

Average Max finds the maximum pressure that was recorded in one of these high-pressure sensels for each cycle of the mannequin's motion. That is, if the mannequin was moved up and down at a frequency of 1.8 Hz, then the averagemax function will find the maximum pressure achieved in each $^{10}/_{18}$ of a second interval and then average all of these values over the whole trial.

This function, like Plot Peak, focuses on sensels that registered above the threshold, so be sure to set the 'peak value' accordingly. Once this is done, click the Average Max button to execute the function.

This data will be displayed in the command window and exported to a spreadsheet file. The file is created in the same directory where the data file is located. It is also named after the data file it was derived from. For example, if the data was from the file 'c:\sab&mike\data.fsx', then the spreadsheet file will be named 'c:\sab&mike\data_avgmx.wk1'.

Average Min

Average Min operates in the same manner as Average Max, but with a few slight differences. It targets the same high-pressure sensels, but instead it averages the MINIMUM pressures from each mannequin cycle.

The output is also the same, except the spreadsheet file is would be named 'c:\sab&mike\data_avgmn.wk1'.

Sensel Average

When you click on the Sensel Average button, the sensel average function calculates mean pressure in each sensel, averaged over the entire trial. This information is displayed in the command window and in a figure. The array containing the mean pressures is also written to a file. Sticking with our 'c:\sab&mike\data.fsx' example, the file would be found with the name 'c:\sab&mike\data_snslavg.wk1'.

Sensel Max

This function acts just like Sensel Average, but it calculates the maximum pressure attained in each sensel during the trial. The output is the same, but the spreadsheet filename will be of the form 'data_snslmx.wk1'.

Centre of Mass

This is actually Mike Eklund's (Centre of Mass or footmov) function with modifications to make it work here. This function calculates the location of the centre of pressure over the entire sensel array for each sample taken in the trial. It then creates a figure showing all the pressures on the array for one frame, as well as the centre of pressure (marked with an X). To display the next frame, the user needs to hit <enter>. To stop showing the frames, the user enters a 0. There are prompts for these keys in the command window.

And that sums up all the actions that can presently be performed by the Manipulator. Any of the figures generated by the functions can be saved by choosing 'Save' from the 'File' menu located at the top of each figure.

CREATING EXCEL SPREADSHEETS

The spreadsheets created by the MATLAB functions are in a format where their meaning is not apparent and their appearance is certainly not presentable. For each of the functions that output a spreadsheet, there is a Visual Basic Macro that converts it into a more useful spreadsheet. These are Macros are contained in the 'thesis_VBmacros.xls' file.

So, when viewing one of the spreadsheets, it is advisable to do so in Excel, with the 'thesis_VBmacros' file open. Then, run the macro that corresponds to the type of function that created the spreadsheet.

QUITTING THE PROGRAM

To exit the program, please select the 'Quit' button located in the bottom right corner of the GUI.

DOCUMENT CONTROL DATA
(Security classification of the title, body of abstract and indexing annotation must be entered when the overall document is classified)

1. ORIGINATOR (The name and address of the organization preparing the document, Organizations for whom the document was prepared, e.g. Centre sponsoring a contractor's document, or tasking agency, are entered in section 8.)

Publishing: DRDC Toronto

Performing: Ergonomics Research Group, School of Physical and Health Education, Queen's Universityy, Kingston, Ontarioo K7L 3N6

Monitoring:

Contracting: DRDC Toronto

2. SECURITY CLASSIFICATION (Overall security classification of the document including special warning terms if applicable.)

UNCLASSIFIED

3. TITLE (The complete document title as indicated on the title page. Its classification is indicated by the appropriate abbreviation (S, C, R, or U) in parenthesis at the end of the title)

Development of a Dynamic Biomechanical Model for Load Carriage: Phase I Part A: Equipment Upgrades to Accommodate Dynamic Biomechanical Modeling (U)

4. AUTHORS (First name, middle initial and last name. If military, show rank, e.g. Maj. John E. Doe.)

Joan M. Stevenson; Susan A. Reid; J. Tim Bryant; Lindsay J. Hadcock; Evelyn L. Morin

5. DATE OF PUBLICATION (Month and year of publication of document.)

August 2005

6a NO. OF PAGES (Total containing information, including Annexes, Appendices, etc.)

74

6b. NO. OF REFS (Total cited in document.)

21

7. DESCRIPTIVE NOTES (The category of the document, e.g. technical report, technical note or memorandum. If appropriate, enter the type of document, e.g. interim, progress, summary, annual or final. Give the inclusive dates when a specific reporting period is covered.)

Contract Report

8. SPONSORING ACTIVITY (The names of the department project office or laboratory sponsoring the research and development − include address.)

Sponsoring:

Tasking:

9a. PROJECT OR GRANT NO. (If appropriate, the applicable research and development project or grant under which the document was written. Please specify whether project or grant.)

12CM03

9b. CONTRACT NO. (If appropriate, the applicable number under which the document was written.)

W7711−0−7632−01/A

10a. ORIGINATOR'S DOCUMENT NUMBER (The official document number by which the document is identified by the originating activity. This number must be unique to this document)

DRDC Toronto CR 2005−115

10b. OTHER DOCUMENT NO(s). (Any other numbers under which may be assigned this document either by the originator or by the sponsor.)

11. DOCUMENT AVAILABILITY (Any limitations on the dissemination of the document, other than those imposed by security classification.)

Unlimited distribution

12. DOCUMENT ANNOUNCEMENT (Any limitation to the bibliographic announcement of this document. This will normally correspond to the Document Availability (11), However, when further distribution (beyond the audience specified in (11) is possible, a wider announcement audience may be selected.))

Unlimited announcement

DOCUMENT CONTROL DATA
(Security classification of the title, body of abstract and indexing annotation must be entered when the overall document is classified)

13. ABSTRACT (A brief and factual summary of the document. It may also appear elsewhere in the body of the document itself. It is highly desirable that the abstract of classified documents be unclassified. Each paragraph of the abstract shall begin with an indication of the security classification of the information in the paragraph (unless the document itself is unclassified) represented as (S), (C), (R), or (U). It is not necessary to include here abstracts in both official languages unless the text is bilingual.)

(U) Part A of Phase I of the contract was to develop the instrumentation so that a dynamic biomechanical model could be developed. The specific objectives were: a) to develop Fastrak™ software for relative pack−person motion, b) construct smaller strap force gauges, c) build and calibrate a moment of inertia platform, d) modify the Load Carriage compliance tester to automate two degrees of freedom and e) create a full body mapping of mannequin. This report describes the purposes and outputs available from the pack−person motion (Section 2.0), describes the development, construction, calibration and protocol for use of smaller strap sensors (Section 3.0) and the moment of inertia platform (Section 4.0), and the development and steps involved in modifying the LC compliance tester (Section 5.0) and the mannequin mapping (Section 6.0). For the most part, tasks were developmental and construction−based with no data analyses, other than to confirm the accuracy and precision of the instrumentation.

This report deals only with Part A consisting of five sub−parts of the contract. Part B involved changing the technical manuals based on the upgrades stated within this report. Part C of this contract is under separate cover and was to develop a long range plan and budget for dynamic biomechanical modeling. Part D was to assist with the NATO HFM Specialist Meeting entitled “Soldier Mobility: Innovations in Load Carriage System Design and Evaluation” held on 27−29 June 2000. Part D is described by the NATO RTO MP−56 Technical Proceedings Report entitled: “Soldier Mobility: Innovations in Load Carriage System Design and Evaluation”.

14. KEYWORDS, DESCRIPTORS or IDENTIFIERS (Technically meaningful terms or short phrases that characterize a document and could be helpful in cataloguing the document. They should be selected so that no security classification is required. Identifiers, such as equipment model designation, trade name, military project code name, geographic location may also be included. If possible keywords should be selected from a published thesaurus, e.g. Thesaurus of Engineering and Scientific Terms (TEST) and that thesaurus identified. If it is not possible to select indexing terms which are Unclassified, the classification of each should be indicated as with the title.)

(U) Load Carriage; Dynamic Biomechanical Modeling; Compliance Tester; Pressure Measurement System; Fastrak™; LC Simulator; Pack−person motion